SOLAR CAR FRONT END SUSPENSION CAPSTONE TEAM

A Final Report submitted to the Department of Mechanical and Aerospace Engineering

University of Virginia • Charlottesville, Virginia

Dhruv Singh, Zachary Wheeden, Christopher Connolly

Ghulamsakhi Mossavi, Jacob Chesley

December 13th, 2024

Capstone Advisor

Dr. Michael Momot, Department of Mechanical and Aerospace Engineering

Technical Advisor

Dr. Tomonari Furukawa, Department of Mechanical and Aerospace Engineering

Table of Contents

Section 1: Problem Statement

The goal of the project is to design and manufacture a front-end suspension system for the UVA Solar Car team. The suspension system consists of a network of components including springs, shock absorbers, pushrods, rocker arms, wishbones, uprights, and mounts, that connect the wheel to chassis. The purpose of the suspension system is to absorb road impacts and maintain tire contact with the ground, providing comfort, stability, and control during driving.

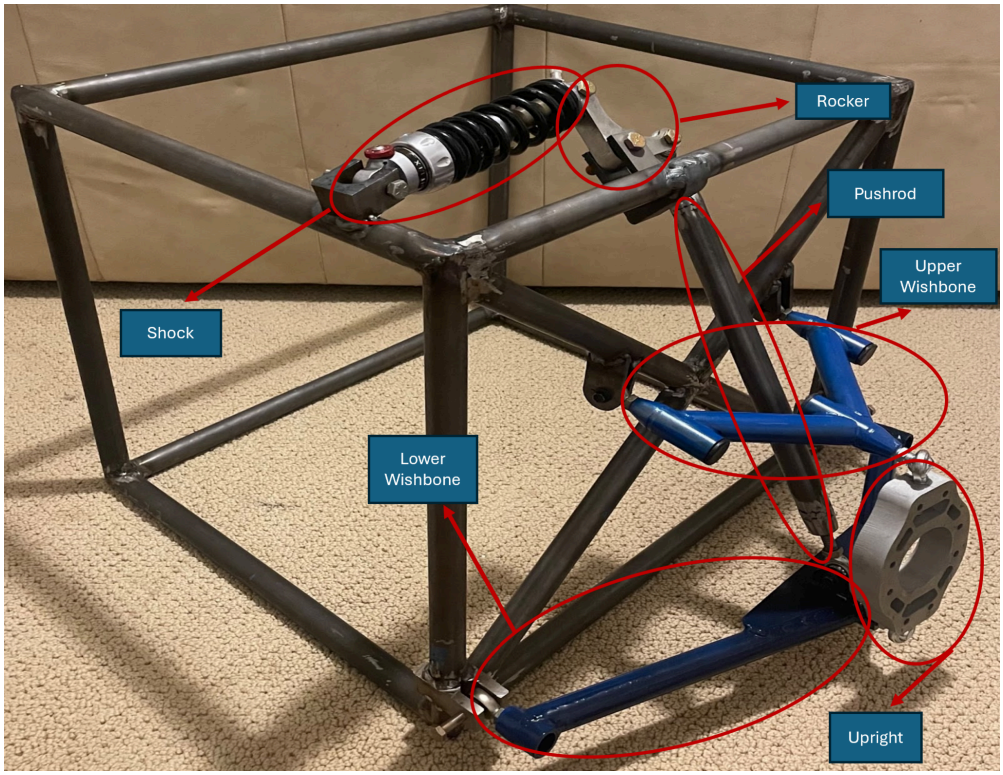

Figure A.1. Suspension system nomenclature

Section 2: Design Process

The team approached the design process with an emphasis on iterative development. Given the time constraints and the manufacturing-intensive nature of the project, the team prioritized identifying and addressing issues early on to avoid significant deviations from the initial design. The team utilized a Gantt chart to schedule and manage design cycle timelines effectively.

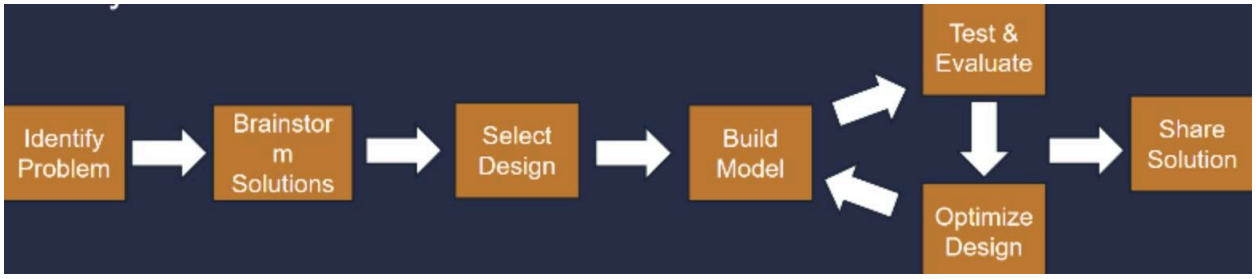

Figure 2: The team implemented an iterative design process, with the majority of effort focused on modeling, testing, evaluation, and optimization

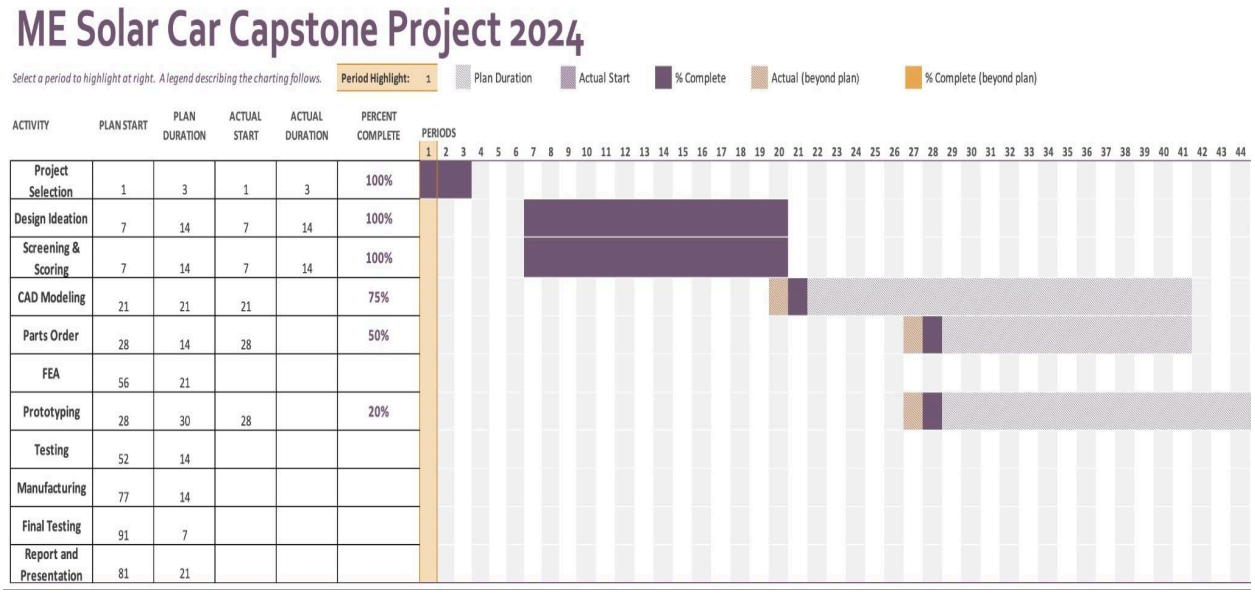

Figure 3: The team used a Gantt chart to manage project scheduling

Section 3: Research

Our team investigated suspension systems of Formula 1 race cars, as well as previous suspension iterations of the UVA Solar Car team. The research focused on incorporating suspension system characteristics from successful Formula 1 vehicles, and avoiding mistakes from previous suspension systems made by the UVA Solar Car team. Additionally, the research concentrated on modular component design, such that specific components such as the shock, rocker, and pushrod can easily be scaled or reconfigured to adapt to changing needs of the vehicle under specific racing conditions.

Research of well-performing suspension systems revealed certain characteristics and qualities that allow for a suspension system to operate efficiently. Examples of these characteristics include: Wishbone shaped control arms, small uprights which housed a large wheel bearing, lightweight steel tubing, and a compact vertical geometry to eliminate bump

steering. There are many more factors that differed between designs that influenced their performance, and through a screening and selection process we narrowed down the specific features the solar car needed tuned for the Formula Sun Grand Prix and American Solar Challenge tracks.

The previous suspension system built by the UVA Solar Car team was insufficient in accomplishing the duties of a properly functioning suspension system. More specifically, the past design poorly mitigated shocks and vibrations due to the incorrect spring rating of the spring damper. The design limited handling and stability of the vehicle because of the large vertical distance between lower and upper control arms, which caused an acute geometry leading to increased vibration and bump steer. A key goal of our research was identifying these causes for poor performance in order to avoid them. Another research goal was to obtain a design that would fit within our specific design limitations of space while still achieving better performance than the previous suspension.

Figure 3: Rivanna 2 Solar car suspension (left) and Chevrolet IndyCar team pushrod suspension (right)

Section 4: Ideation

The team developed a wide variety of initial design concepts for a suspension system that could accomplish the project goal. These ideas included traditional, advanced designs, as well as unorthodox concepts. A few of the considered designs are included on the following page.

a. Double Wishbone Pushrod:

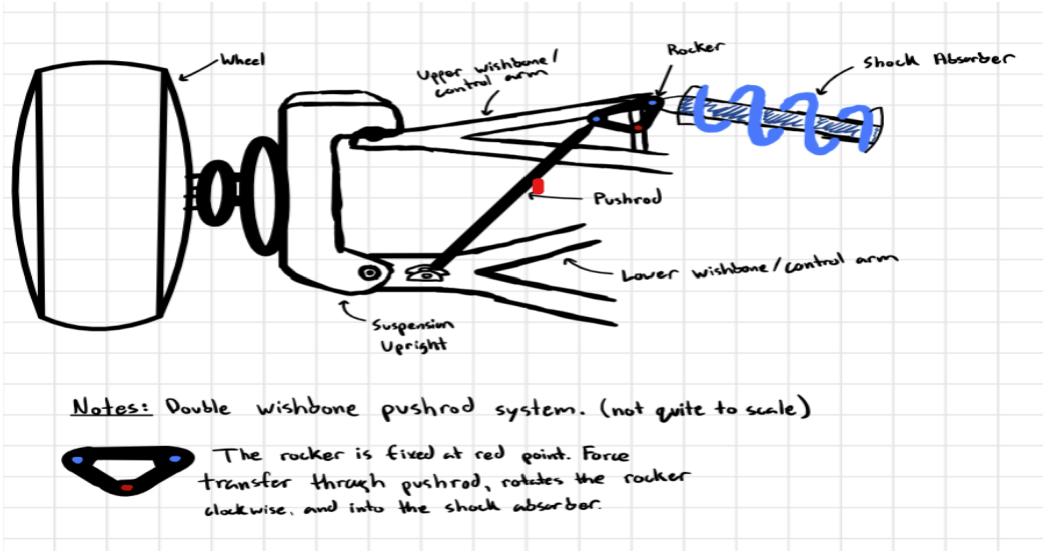

Figure 4: The double wishbone suspension configuration is able to translate vertical displacement of the wheel into horizontal displacement of the shock via a pushrod and angled rocker

b. Connected Pushrod with 3 Dampers:

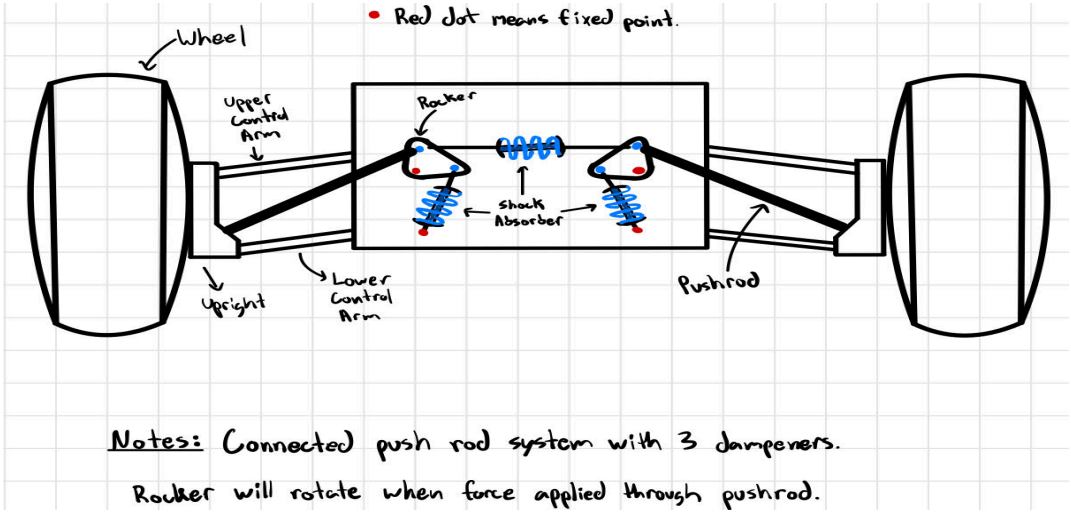

Figure 5: The connected pushrod with 3 dampers is similar to design A, with an added damper between both the two rockers, enhancing suspension control

c. Double Wishbone 90 Degree Pushrod:

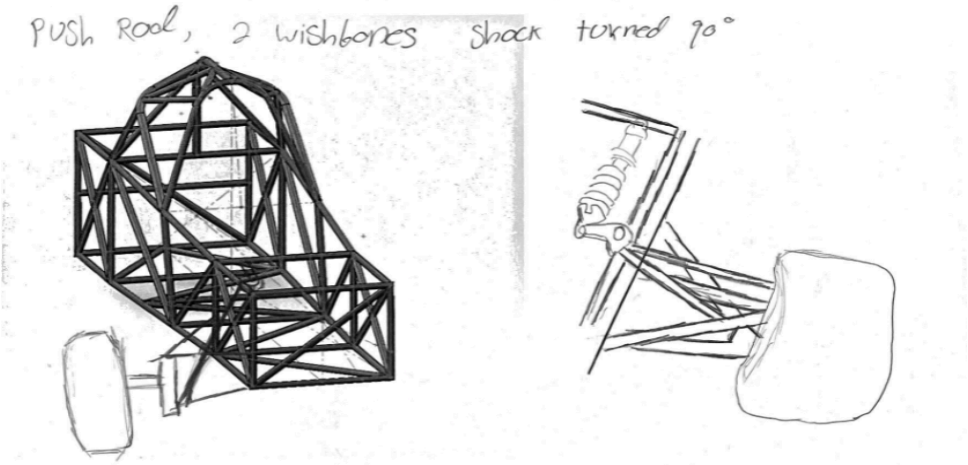

Figure 6: The double wishbone with the pushrod is similar to design a, with the shock mounted in line with the longitudinal axis of the vehicle

d. Flexible Wishbone

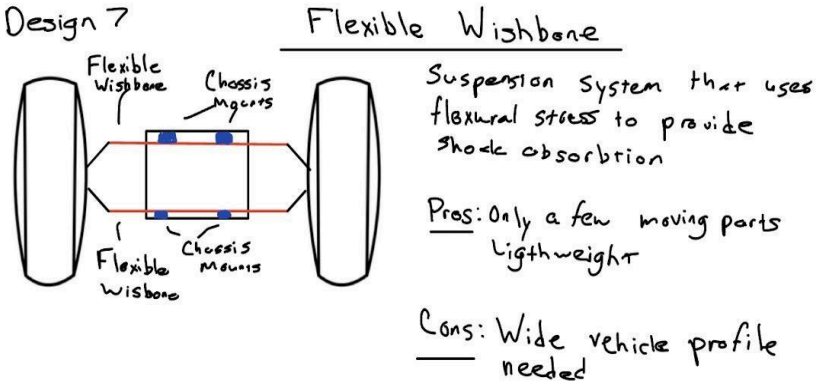

Figure 7: The flexible wishbone design utilizes bending resistance in lieu of conventional springs to absorb energy. The flexible wishbones do not have a mechanism to control damping, meaning the suspension system is not easily tunable

e. Elastic Material Damping

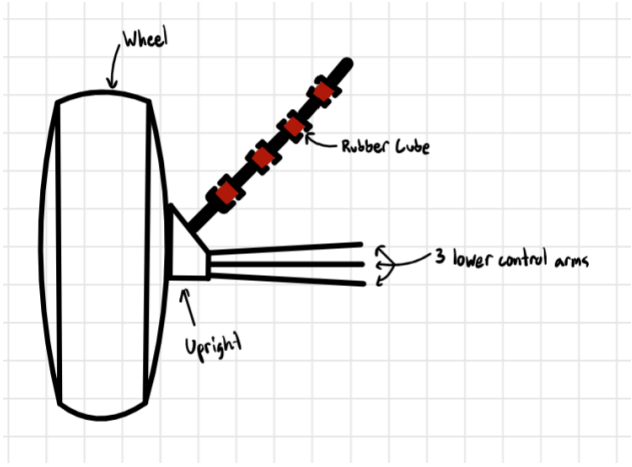

Figure 8: The elastic material dampener is an unconventional suspension method that utilizes materials such as rubber to dissipate energy

Selection and Screening

In the engineering design process, creating many ideas was crucial as to give a plethora of options to choose from. With all these options on the table, the following criteria guided the design selection, weighted based on importance:

Selection Criteria:

- ➔ **Ride Characteristics (30%):** Ability to maintain stable and predictable handling, including smooth cornering and consistent braking. Weighting was prioritized due to the critical role of ride dynamics in both racetrack performance and cross-country stability.
- ➔ **Ease of Manufacture (15%):** Practicality and cost of production, considering tools, materials, and machining techniques. This criterion was weighted to ensure the design could be fabricated within time and resource constraints.
- ➔ **Ease of Maintenance (15%):** Accessibility for repairs and adjustments with minimal disassembly required. Maintenance was given significant weight to reduce downtime and enhance reliability.
- ➔ **Creativity (10%):** Innovation in design, fostering new methods to solve traditional suspension challenges. Creativity was included to encourage forward-thinking and novel solutions.
- ➔ **Weight (10%):** Reduction to improve efficiency, ensuring a lightweight design without compromising strength. Weight was prioritized to minimize energy consumption and maximize solar efficiency.

- ➔ **Durability/Fatigue Life (10%):** Longevity under repeated dynamic loads, especially during high-stress conditions. Ensuring the system's durability was critical to avoid failures during long races.
- ➔ **Adjustability (5%):** Ability to adapt to different scenarios, such as varied track surfaces and weight distributions. Adjustability was weighted lower as it is a secondary consideration compared to core performance.
- ➔ **Profile Dimensions (5%):** Compatibility with the Solar Car's chassis, requiring a low-profile and compact design to fit space constraints. While important, dimensional constraints were weighted lowest as all designs inherently adhered to these requirements.

Table 1: Pugh Matrix

	Concept Variants								
Selection Critera	A	B	C	D	E	F	G	H	Reference
Ride Characteristics	1	1	1	1	1	0	1	0	0
Ease of manufacture	0	-1	-1	1	-1	0	0	-1	0
Ease of maintenance	1	-1	-1	1	-1	1	1	-1	0
Creativity	1	1	1	1	1	1	1	1	0
Lightweight	1	0	0	0	0	1	1	1	0
Durability	0	1	0	-1	1	1	0	-1	0
Adjustability	1	1	0	0	1	1	1	-1	0
Low Profile	1	1	0	1	1	1	1	1	0
Sum	6	3	0	4	3	6	6	-1	0
Proceed	Yes	No	No	No	No	Yes	Yes	No	N/A

A	Double Wishbone Pushrod
B	Connected Pushrod W/ 3 Dampers
C	Connected Spring
D	Single Wishbone In-line Pushrod
E	Single Control Arm Connected Springs
F	Cantilever Suspension
G	Double Wishbone 90 Degree Pushrod
H	Flexible Wishbone

Screening Process:

Initial concepts were scored against a baseline reference (Rivanna 2 suspension) using a Pugh Matrix. Each concept was evaluated on the selection criteria:

- ➔ **+1**: Improvement over the reference.
- ➔ **0**: No significant difference.
- ➔ **-1**: Regression compared to the reference.

This process eliminated designs that failed to demonstrate substantial advantages or exhibited significant drawbacks. Concepts like the Single Control Arm Connected Spring were discarded early due to limited adjustability and suboptimal ride characteristics.

Weighted Decision Matrix:

The top three designs from the Pugh Matrix evaluation were reanalyzed using a weighted decision matrix to quantify performance based on the selection criteria. The weighted scores were calculated as follows:

Table 2: Weighted Decision Matrix

	Concepts								
		A		F		G		Reference	
Selection Critera	Weight	Rating	Weighted	Rating	Weighted	Rating	Weighted	Rating	Weighted
Ride Characteristics	30%	5	1.5	3	0.9	5	1.5	3	0.9
Ease of manufacture	15%	3	0.45	3	0.45	2	0.3	3	0.45
Ease of maintenance	15%	4	0.6	4	0.6	4	0.6	3	0.45
Creativity	5%	5	0.25	5	0.25	5	0.25	3	0.15
Lightweight	10%	4	0.4	4	0.4	4	0.4	3	0.3
Durability	10%	3	0.3	4	0.4	3	0.3	3	0.3
Adjustability	5%	5	0.25	5	0.25	5	0.25	3	0.15
Low Profile	10%	5	0.5	5	0.5	5	0.5	3	0.3
Total Score			4.25		3.75		4.1		3
Rank			1st		3rd		2nd		4th

A	Double Wishbone Pushrod
F	Cantilever Suspension
G	Double Wishbone 90 Degree Pushrod

Weighted decision matrix

The double wishbone pushrod ranked highest due to its strong performance in critical categories such as ride characteristics, ease of maintenance, and adaptability. The cantilever suspension, while excelling in weight reduction, lacked the structural integrity and adjustability necessary for high-performance scenarios. The double wishbone 90 degree pushrod also scored strongly in each of the categories, though its total score was slightly lower than the double wishbone pushrod. Between the top two designs, our team determined the final design to be the double wishbone 90 degree pushrod. Although this concept wasn't the top scoring design, our team had a personal preference for this design, in addition to it scoring very similarly to the top design.

Section 5: Initial Specifications

Since the vehicle is still in the design phase and definitive specifications such as weight and rear-to-front wheel load distribution are unavailable, our team made reasonable assumptions to define the suspension requirements ahead of the car's design. These assumptions are based on historic vehicle data, including solar car data from previous years, which follows a consistent trend. The key vehicle parameters and their corresponding values are listed below.

Total Vehicle Weight with Driver: 720 lb

Sprung Vehicle Weight: 600 lb

Unsprung Mass: 120 lb

Ride Height: 4 in.

Max Allowable Wheel Travel: 3.61 in.

Outer Clearance Limit: 29in from center of chassis

Inner Clearance Limit: 11in from center of chassis

Minimum Turn Radius: 8 meters

Minimum Ride Height: 4 inches

Tables 3 and 4 were developed to standardize and quantify the importance of vehicle suspension requirements and corresponding performance metrics.

Table 3: Requirements Importance Quantification

#	NEED	Imp
1	Suspension increases grip of wheels to track	5
2	Suspension reduces vibration to the driver	3
3	Suspension increases handling around turns	4
4	Suspension enables high speed descents on bumpy trails	5
5	Suspension is lightweight	3
6	Suspension provides stiff mounting points for the brakes	5
7	Suspension can be easily accessed for maintenance	3
8	Suspension accounts for steering geometry and integrates tie rods into designs.	4
9	Take measures to prevent bump steer while traveling	4

Table 4: Requirements Standardization

Metric #	Need #s	Metric	Imp	Units
1	1, 2	Vibration attenuation to the driver at 10 Hz	3	dB
2	2, 3	Maximum vertical travel over rough terrain	5	in
3	3, 4	Lateral stability during cornering	4	lb-f
4	1, 5	Steering responsiveness adjustment range	3	lbf-s/ft
5	4, 6	Maximum impact absorption at high speed descents	5	g
6	7	Total weight of the suspension system	4	lbm
7	5	Ground clearance during compression	3	in
8	8	Lateral stiffness at critical mounting points	4	lbf/ft
9	6	Time to adjust suspension settings	2	s
10	5, 9	Compatibility with different wheel sizes	5	list
11	10	Ease of assembly to chassis	1	s
12	16	Time to disassemble/assemble for maintenance	3	s
13	17, 18	Special tools required for maintenance	3	list
14	18	Suspension lifespan under normal operating condition	5	cycles
15	19	Maximum bump steer correction during travel	4	degrees
16	12	Subjective feedback on pride and aesthetics	5	subjective
17	3, 5	Maximum descent time over bumpy tracks	5	s
18	14	Resistance to contamination (water, mud, etc).	5	binary

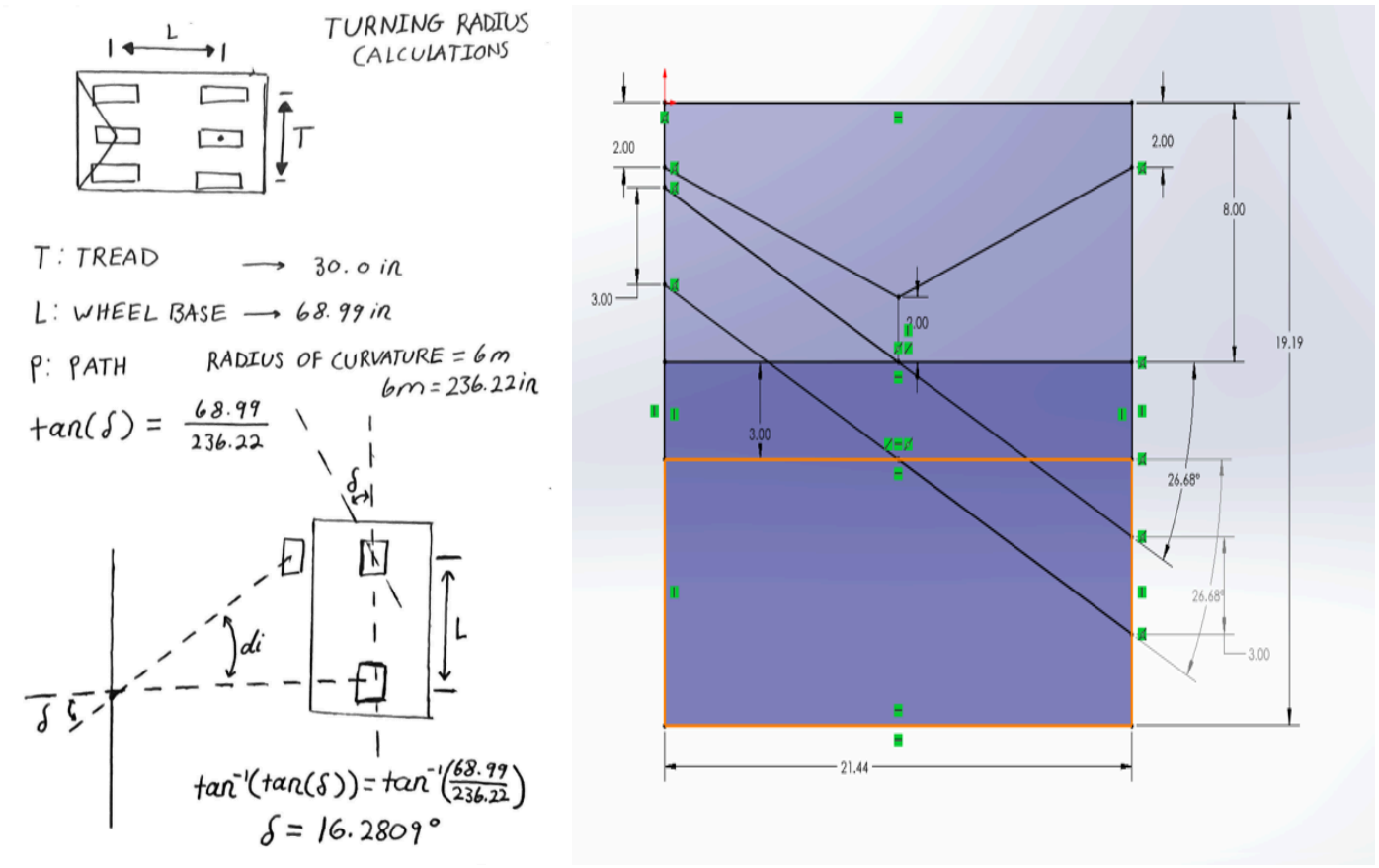

Figure 9: Calculations and Geometric Models Showing The Necessary Steering Angle Of 16.28 Degrees (Left) and Achieved Steering Angle Of 26.86 Degrees(Right)

Turning radius was also a large factor in component design. Due to the narrow space between the aeroshell of the solar car and the chassis, the geometry was forced into a tight space making steering angles limited. By the solar car regulations we must be able to navigate the car within a 6 meter turning radius. With this specification in place, the design was made to have at least 16,3 degrees of steering angle, but through the sketch above we see that our suspension system archives 26.68 degrees of steering angle. This validates our model and allowed us to continue designing from there.

One of the biggest challenges, aside from the lack of definitive specifications, is designing for the expected routes the vehicle needs to navigate, specifically, a race track and an extensive 1500 mile road course. The demands of the racetrack, with its tight corners and rapid acceleration, contrast sharply with those of a cross-country race, which emphasize long-term vehicle durability and driver endurance. To develop a suspension system capable of operating in these race conditions, we designed a modular system that can easily accommodate new components-such as shocks, dampers, or rocker mounts with different lever ratios-allowing us to

adjust vehicle dynamics to better suit the environment without requiring a major redesign of the suspension system.

Prototyping

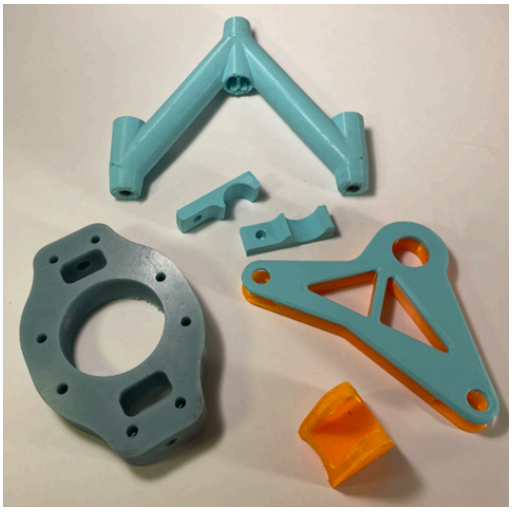

Figure 10: 3D Printed Prototype Components

Figure 11: Creality CR-10 Smart Printer

Figure 12: Elegoo Saturn Resin Printer

The prototyping process consisted of modeling and 3D printing the individual components of the assembly. Components bearing less stress were printed using Fused Deposition Modeling (FDM) and those taking more stress were printed in resin. The images above show the 3D printers used in this process, for FDM printing, the Creality CR-10 Smart was used due to the large printer bed size, allowing the fabrication of our larger components such as the wishbones and rockers. The printer used to fabricate stronger, more dense components is an Elegoo Saturn resin printer that handled components such as the upright.

Section 6: Testing

Given the inability to test the suspension system as a complete unit, we focused on evaluating individual components and simulating overall performance. Laboratory testing and finite element analysis (FEA) were used to assess component performance and safety. To analyze the system's dynamic behavior under road inputs, a Simulink quarter-car model was developed to simulate its response.

Finite element analysis (FEA) is an exemplary method of predicting mechanical failure in a component without having to manufacture the computer-aided designs. We chose to conduct static structural simulations including a safety factor to ensure the parts won't fail under continuous loading. The process of FEA involves creating an appropriate mesh layout, applying the loads and boundary conditions, and solving the system for the desired results. We were most interested in finding the maximum stress, strain, and deformation values to compare them to the component's inherent material properties (Figure C.17 & C.18).

Meshing creates a grid of encompassing elements that are individually evaluated by a complex mathematical algorithm relative to each other. The mesh settings that applied to all components include a quadratic mathematical model for the most robust calculations and tetrahedron geometry for every mesh element. The first FEA results obtained are usually inaccurate due to constraints in the size of the meshing. After obtaining the initial results and locating the faces with high stress concentrations, the mesh size would then be refined on those specific faces by integer multitudes. The system would then be solved recurrently until the maximum stress (or any other result) converges within reason on a final value. The default size of each element ranged from three to five millimeters, but this was only to account for a node limit placed on the free, student version of Ansys. Refinement of the element size on significant locations was deemed more important than the default size of the elements themselves. Below is an example of the final 3mm meshing of the rocker with three times refinement on the locations of applied force and two times refinement on the face connecting to the rocker mount (Figure 13).

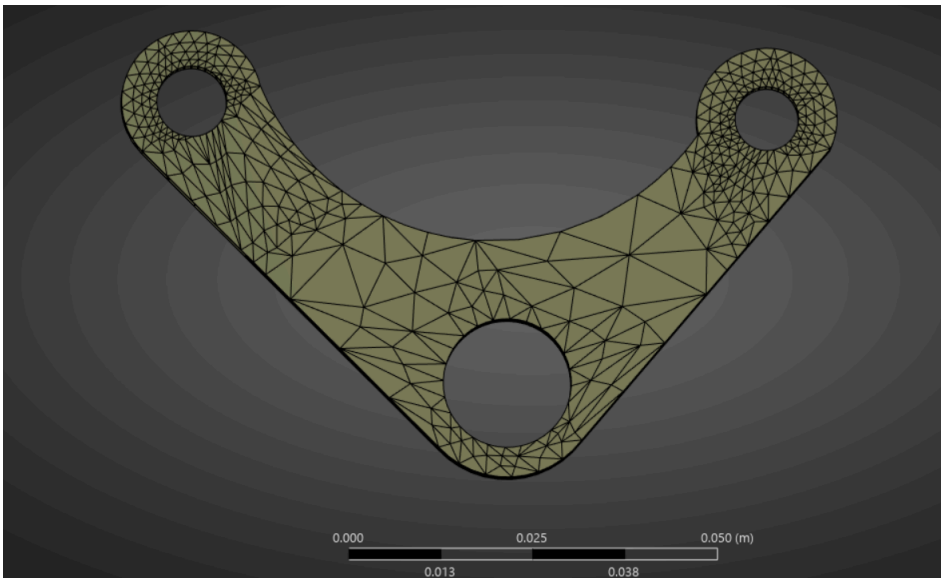

Figure 13. Final rocker mesh using refinement

The loading and boundary conditions had to be applied to each part with careful consideration. Using coordinates of the connections and vector notation for the lines of action was a simple way to ensure the forces were applied in the proper directions. Generally, the motion constraints are located at the connections to parts of the car not included in the suspension system such as the chassis or wheel. For example, the upright has a displacement constraint that restricts all rotational motion connection to the wheel as well as all translational motion except up and down (Figure 14). A second cylindrical boundary condition was then applied to the hole connecting the upper wishbone. This allowed a bearing load to be applied to the center of the upright originating from the normal force of the tire. The loading applied to the upright is simply half the weight of the car (360lbs, considering a complete load transfer during maximum cornering) times a safety factor of five. Some components were tested using the maximum force of the spring given the spring constant (400lb/in) and maximum displacement (2.4in) since the spring is the only applied force acting on those parts and no terrain will ever cause the spring to fully compress.

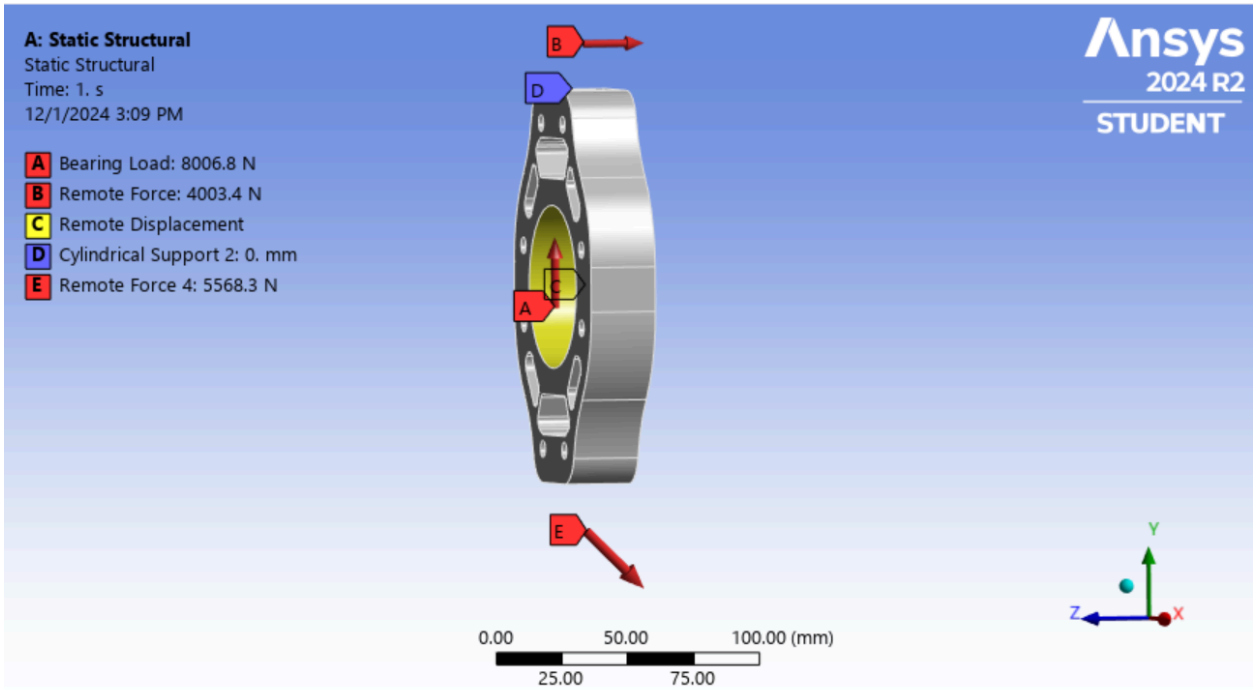

Figure 14. Upright Force Analysis

The final stress concentrations were compared with the yield strengths of the material we decided to go with for each part to ensure no plastic deformation or fracture would occur. A detailed analysis of the FEA of each component can be found in total in Appendix C.

Lab Testing

A compression test was performed on the spring damper using an Instron machine to determine spring rate and maximum deflection. The test revealed a spring rate of approximately 400 pounds per inch and a maximum deflection of 2.4 inches. These values are favorable for racetrack conditions, where a relatively larger spring rate allows for increased responsiveness and handling efficiency.

Figure 14: The Instron pneumatic materials testing device was used for compression testing to verify spring rate and maximum deflection. The spring and maximum deflection were measured to be in accordance with manufacturers specifications at $k = 400\ lb/in$ *and* $\delta = 2.4\ in$

Dynamic Response Analysis

The system's dynamic response was simulated using a parameterized Simulink model, which represents the transient behavior of a quarter-car suspension system. The model incorporates key parameters such as wheel and shock spring coefficients, damper coefficients, damping ratio, and sprung and unsprung weights. While the parameter values are predefined, the model offers an efficient platform to explore how variations in these parameters influence system performance.

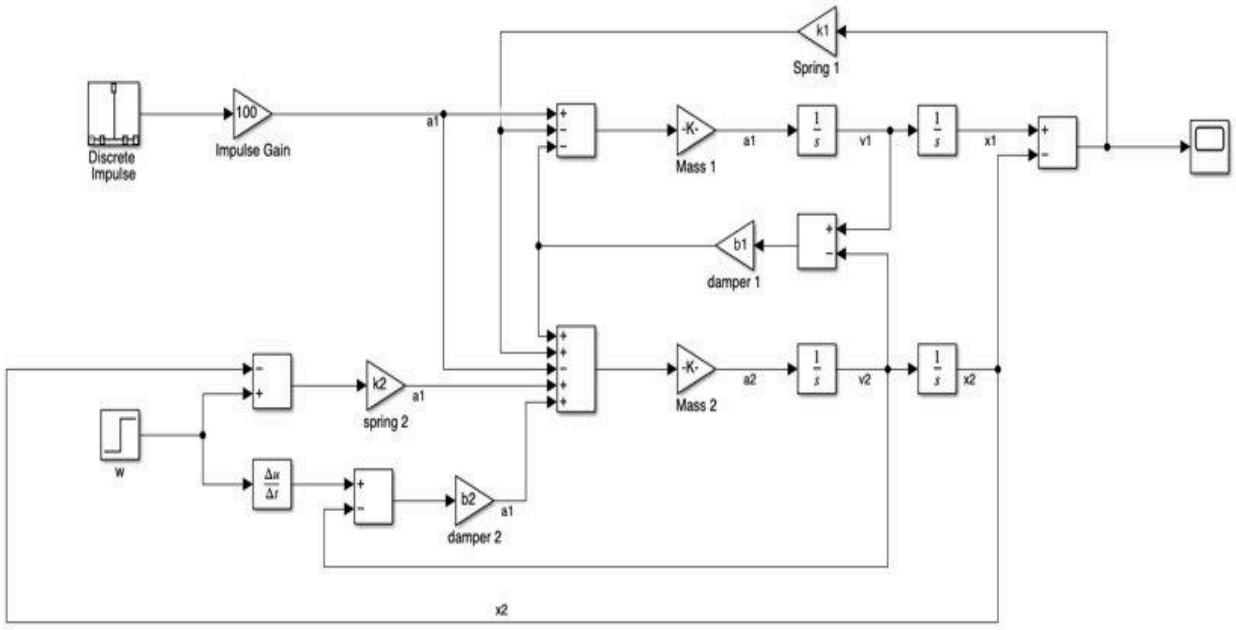

Figure 15: The parameterized Simulink model that computes and displays the transient response of the system given a discrete impulse, representative of a disturbance on the road such as a bump. The input signal for the model can be customized to represent specific race courses or road conditions, allowing for a more accurate simulation of real-world operating environments

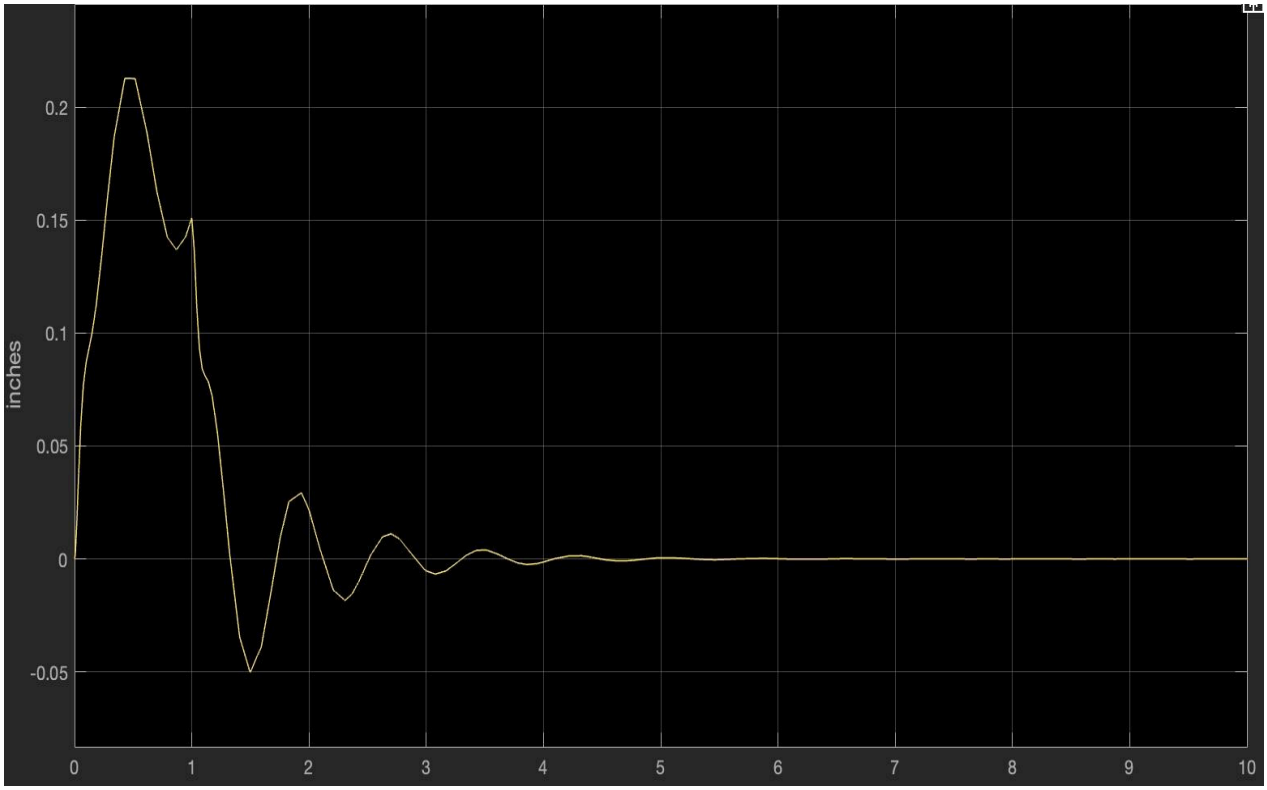


```
m1 = 5.59; %Sprung Mass in slugs
m2 = .931; %Unsprung Mass in slugs
k1 = 600; %Spring Constant in lb/in
k2 = 800; %Tire Spring Coefficient in lb/in
damping_ratio = .4; %damping ratio
b1 = 2*damping_ratio*sqrt(k1*m1); %Shock Damping Coefficient in lb*s/in
b2 = 2; %Tire Damping Coefficient in lb*s/in
```

Figure 16: Transient responses of the system given an impulse input. The model parameters are approximations, chosen to be relatively realistic in the absence of exact values

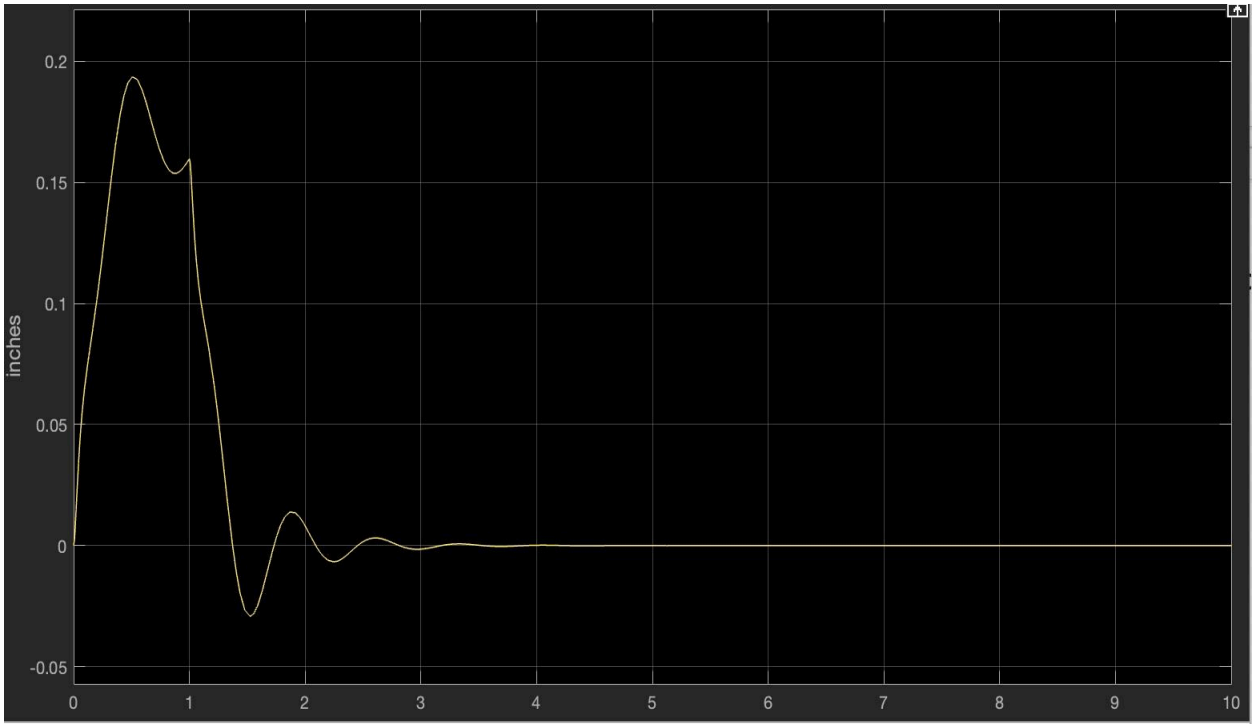


```
m1 = 5.59; %Sprung Mass in slugs
m2 = .931; %Unsprung Mass in slugs
k1 = 600; %Spring Constant in lb/in
k2 = 800; %Tire Spring Coefficient in lb/in
damping_ratio = .7; %damping ratio
b1 = 2*damping_ratio*sqrt(k1*m1); %Shock Damping Coefficient in lb*s/in
b2 = 2; %Tire Damping Coefficient in lb*s/in
```

Figure 17: Transient response of the system given an impulse input. The parameters for the vehicle in both simulations are the same with the exception of the damping ratio. The damping ratio in the first simulation, 0.4, is a less aggressive damping factor and is more reflective of the suspension damping ratio in a sports car. The higher damping factor in the second simulation, 0.7, is more representative of racecar. As expected, the transient responses demonstrated that the higher damping factor led to a faster system settling time.

Results

The team successfully designed and manufactured a fully articulating pushrod suspension system demonstration model. The test assembly allows for adjustments to wheel camber, toe, and wheelbase by repositioning the threaded points on the wishbone. The vertical displacement of the upright, which serves as a proxy for the wheel, met the goal of a maximum allowable vertical displacement.

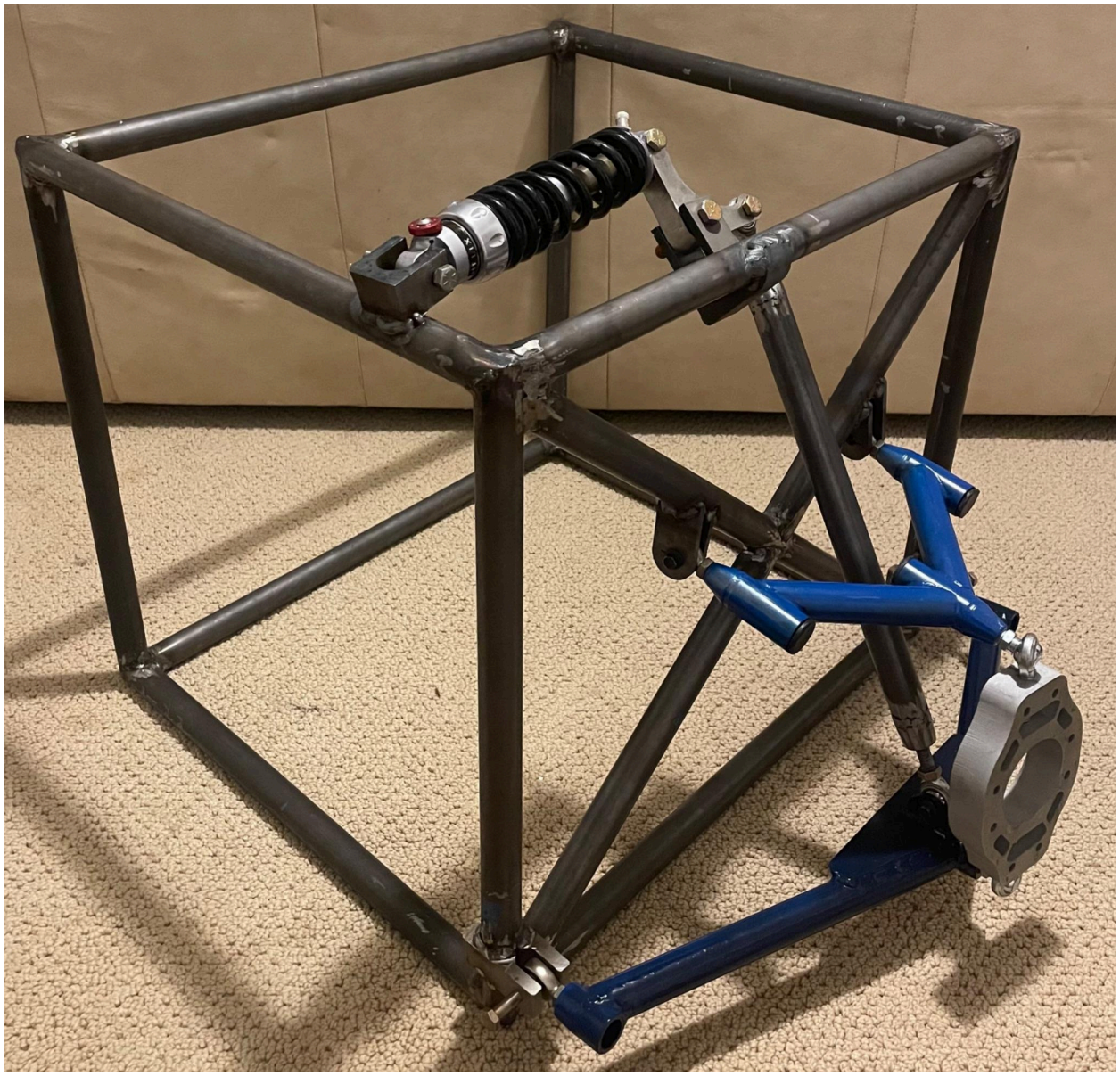

Figure 16: Isometric view of the final project design of the suspension demonstration unit. The demonstration unit fully articulates. The dynamic response of the system can be tuned by adjusting the rocker arm ratio and or the shock. The geometric layout can be reconfigured by adjusting the threaded attachment joints on the upper and lower rocker mounts, as well as the pushrod attachment ends

Figure 17: Front view of the suspension system. The upright has slots cut out to reduce weight

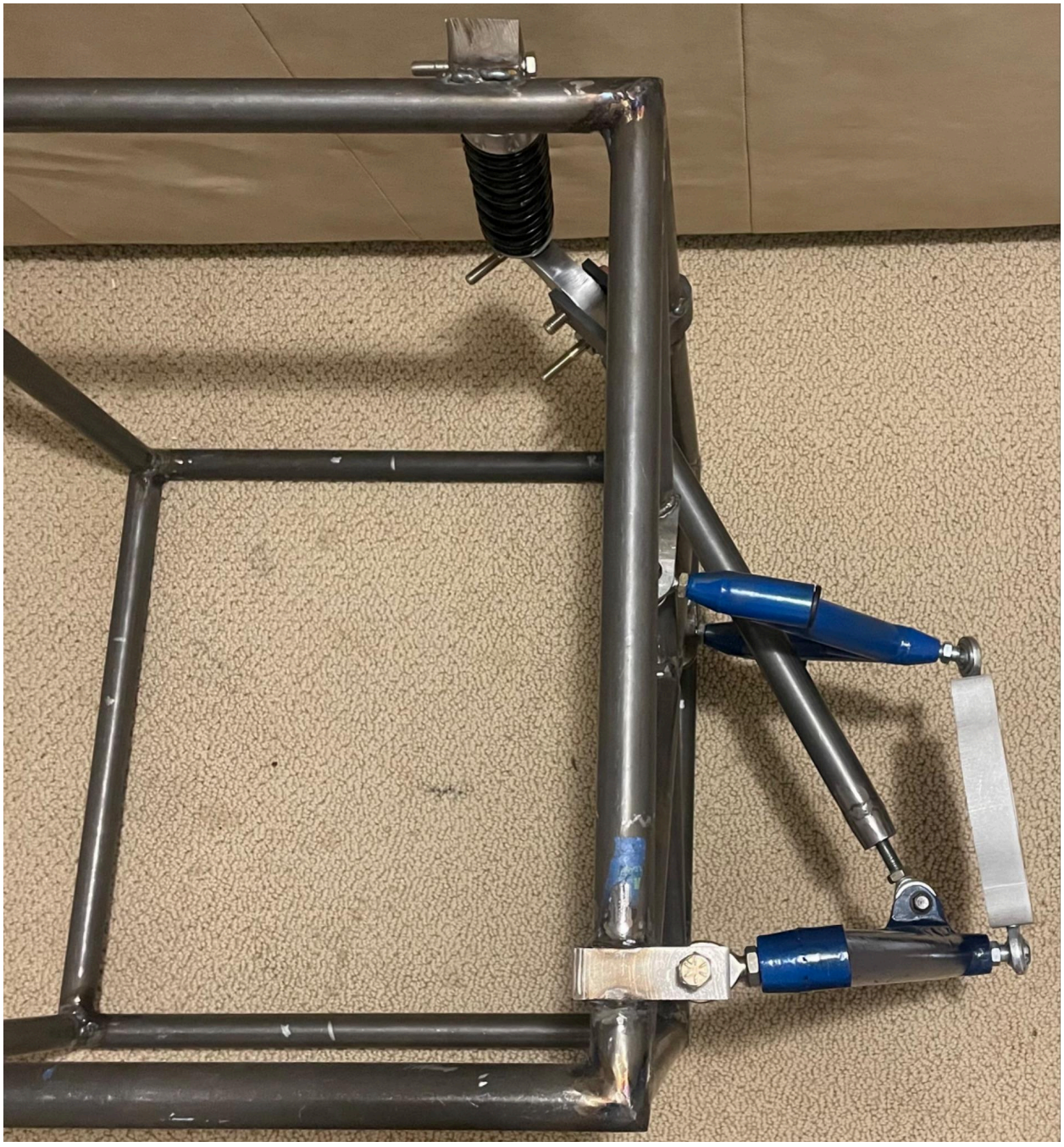

Figure 18: Profile view of the suspension system. The compact width of the suspension system is a critical characteristic, as the wheelbase must fit entirely inside of the aeroshell

Section 7: Summary and Conclusion

The UVA Solar Car Front End Suspension Capstone project represents a comprehensive engineering design process aimed at creating an innovative and high-performance suspension system for a solar-powered vehicle. The team's approach was methodical and thorough, addressing the complex challenges of designing a suspension system capable of performing effectively in both racetrack and cross-country racing conditions.

The project began with a clear problem statement: to design and manufacture a front-end suspension system demonstration unit that would serve as both a proof of concept and a test unit for the UVA Solar Car team. The team's research was extensive, drawing insights from Formula 1 racing suspension systems and learning from previous iterations of the UVA Solar Car team's designs. This approach allowed them to identify key design characteristics such as wishbone-shaped control arms, lightweight steel tubing, and a compact vertical geometry.

A critical aspect of the project was the comprehensive design selection process. The team developed multiple initial concepts and employed a rigorous screening methodology using a Pugh Matrix and a Weighted Decision Matrix. They established a nuanced set of selection criteria, with ride characteristics receiving the highest priority (30%), followed by ease of manufacture and maintenance. This systematic approach ensured that the final design would not only perform well but also be practical to produce and maintain.

The Double Wishbone Pushrod design emerged as the optimal solution, distinguished by its superior performance across critical categories. The team's innovative approach included developing a modular system that could be easily adapted to different racing conditions, addressing the significant challenge of designing for both tight racetracks and long-distance road courses.

Extensive testing and analysis were conducted to validate the design. Laboratory testing of the spring damper and dynamic response analysis using a Simulink quarter-car model provided insights into the suspension system's performance. Finite Element Analysis (FEA) was used to evaluate individual components, examining stress distribution, deformation, and safety factors for critical parts like the rocker mount and upright.

The FEA results revealed valuable insights into the structural integrity of the suspension components. While most analyses showed minimal deformation and stresses within acceptable ranges, they also highlighted potential areas for optimization, particularly around mounting holes and connection points.

Key project achievements include:

- A modular suspension design adaptable to different racing conditions
- Improved performance compared to previous iterations
- Comprehensive analysis of component performance
- Consideration of multiple design constraints and performance criteria

The project's most significant contribution is a suspension system that balances multiple critical requirements: ride characteristics, manufacturability, maintenance ease, weight reduction, and durability. By creating a flexible, well-engineered solution, the team has provided the UVA Solar Car team with a robust foundation for future vehicle development.

Looking forward, the team recommends continued iterative design, further testing under various conditions, and potential refinements to areas identified in the FEA as having stress concentrations. This project exemplifies the power of systematic engineering design, demonstrating how careful research, creative problem-solving, and rigorous analysis can produce innovative technical solutions.

Section 8: Appendix

Appendix Section A: Bibliography

Bayer, A. (n.d.). *Adjustable pushrod suspension system*.

Chauhan, P., Sah, K., & Kaushal, R. (2021). Design, modeling and simulation of suspension geometry for formula student vehicles. *Materials Today: Proceedings*, *43*, 17–27. https://doi.org/10.1016/j.matpr.2020.11.200

Control Tutorials for MATLAB and Simulink—Suspension: Simulink Modeling. (n.d.). Retrieved November 28, 2024, from https://ctms.engin.umich.edu/CTMS/index.php?example=Suspension&section=SimulinkModeling

Milliken, W. F., & Milliken, D. L. (1995). *Race Car Vehicle Dynamics*. SAE International.

Revoor, S., Nikhil, M., & Anil, J. (2019). Design and Modeling of Pull Rod and Push Rod Suspension System. *International Journal of Trend in Scientific Research and Development*, *Volume-3*, 1074–1077. https://doi.org/10.31142/ijtsrd23263

Russell, T. C. (n.d.). *The properties of Bridgestone Ecopia solar car tires (for the UMR solar car team)*.

Appendix Section B: Billing

Date	Requester Name	Supplier	Item	Link to Item	Part/Model #	Price per Unit (and length if needed)	Quanity Desired	Worktag (ALL grants and projects must have an assignee)	Shipping Address
10/29/2024	Momot/Singh	McMaster-Carr	Steel Tubing	https://www.mcmaster.com/89955K6		$48.62	6	MAE 4610: ME Design I (Capstone engineering project)	Mike Momot 122 Engineer's Way Mechanical Engineering, University of Virginia Charlottesville, VA 22903
10/30/2024	Momot/Singh	McMaster-Carr	Tube-end weld nut	https://www.mcmaster.com/products		$8.02	20	MAE 4610: ME Design I (Capstone engineering project)	Mike Momot 122 Engineer's Way Mechanical Engineering, University of Virginia Charlottesville, VA 22904
10/31/2024	Momot/Singh	McMaster-Carr	Ball Joint Linage	https://www.mcmaster.com/60645K2		$10.10	4	MAE 4610: ME Design I (Capstone engineering project)	Mike Momot 122 Engineer's Way Mechanical Engineering, University of Virginia Charlottesville, VA 22905
11/1/2024	Momot/Singh	McMaster-Carr	1/8th in Sheet Metal steel	https://www.mcmaster.com/6863N6-		$78.64	2	MAE 4610: ME Design I (Capstone engineering project)	Mike Momot 122 Engineer's Way Mechanical Engineering, University of Virginia Charlottesville, VA 22906
11/2/2024	Momot/Singh	McMaster-Carr	24"x4"x3" Aluminum Stock	https://www.mcmaster.com/89155K3		$312.38	1	MAE 4610: ME Design I (Capstone engineering project)	Mike Momot 122 Engineer's Way Mechanical Engineering, University of Virginia Charlottesville, VA 22907
	Total					$457.76			

Figure C.1: Bill of materials

Appendix Section C: Drawings

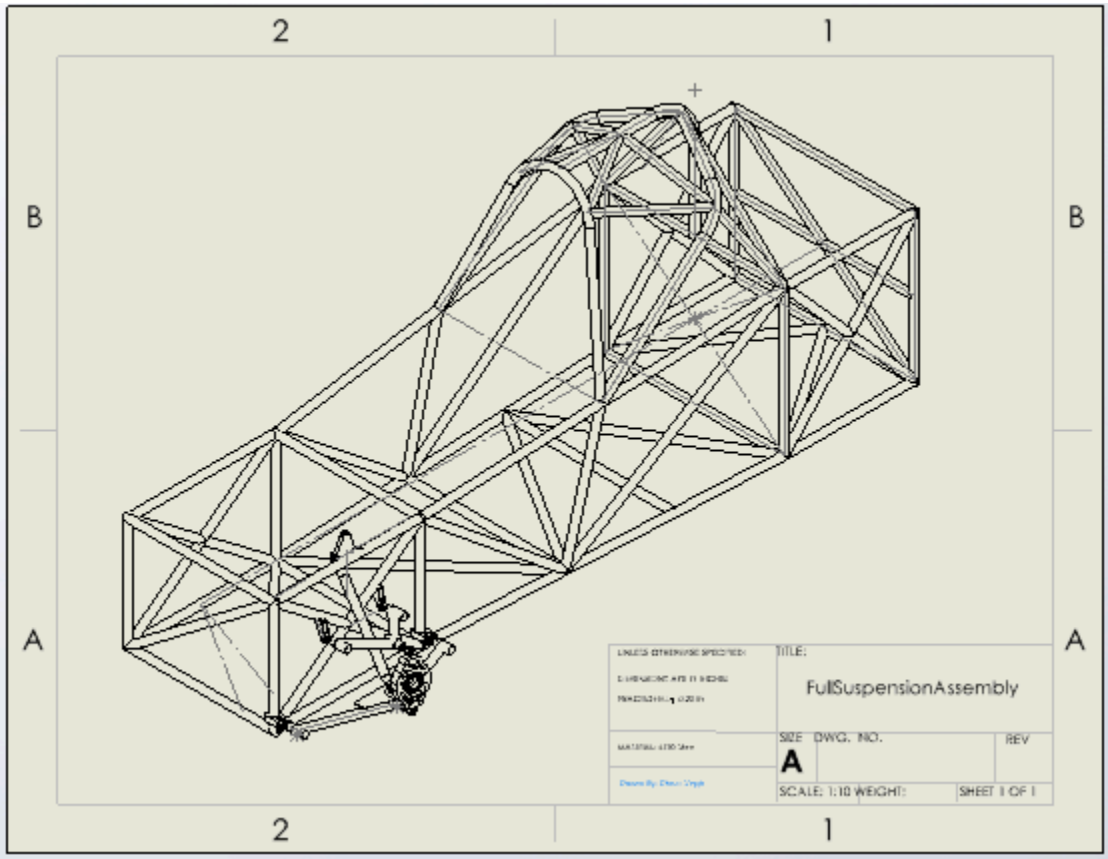

Figure C.1: Full Suspension Assembly Drawing

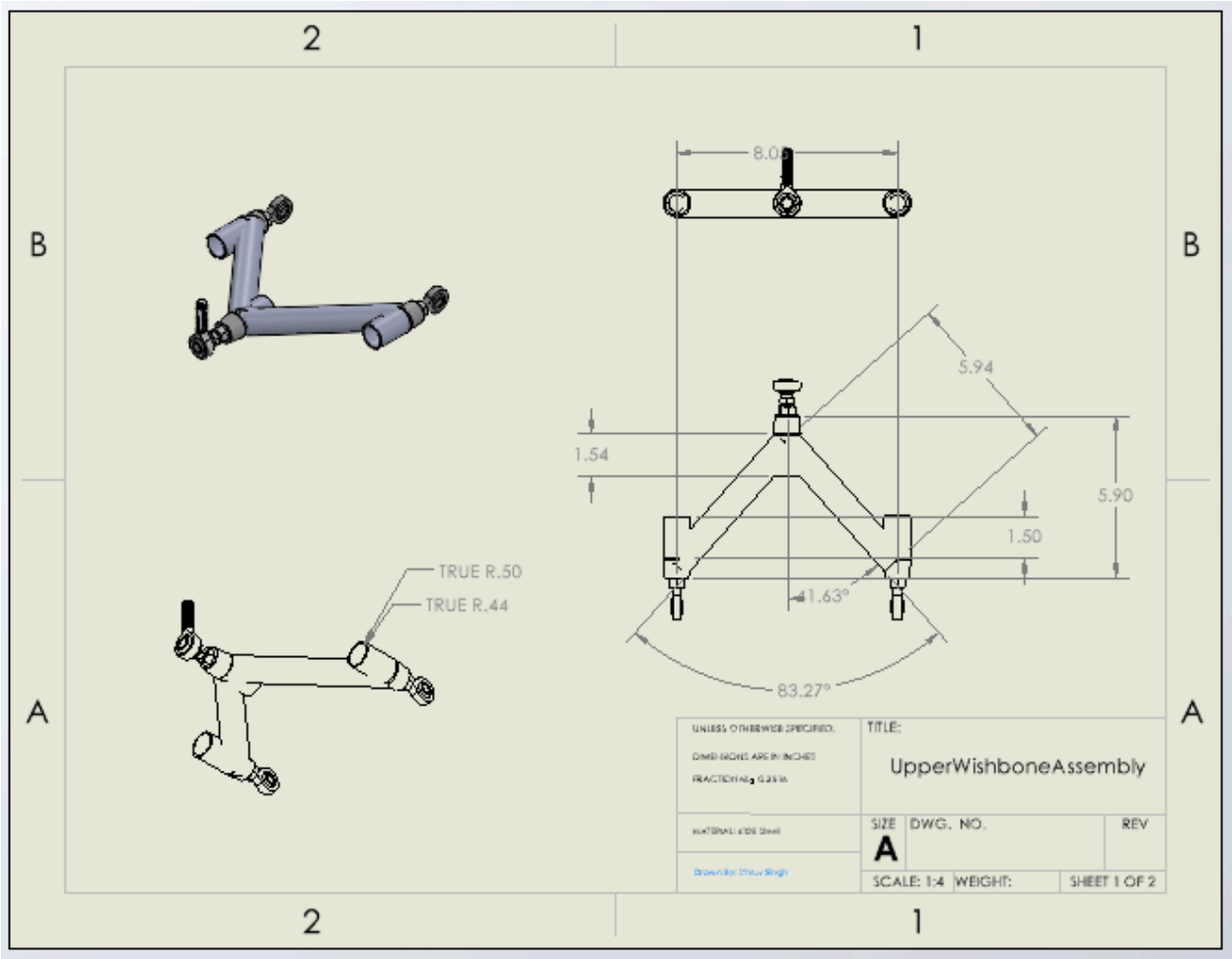

Figure C.2: Upper Wishbone Assembly Drawing

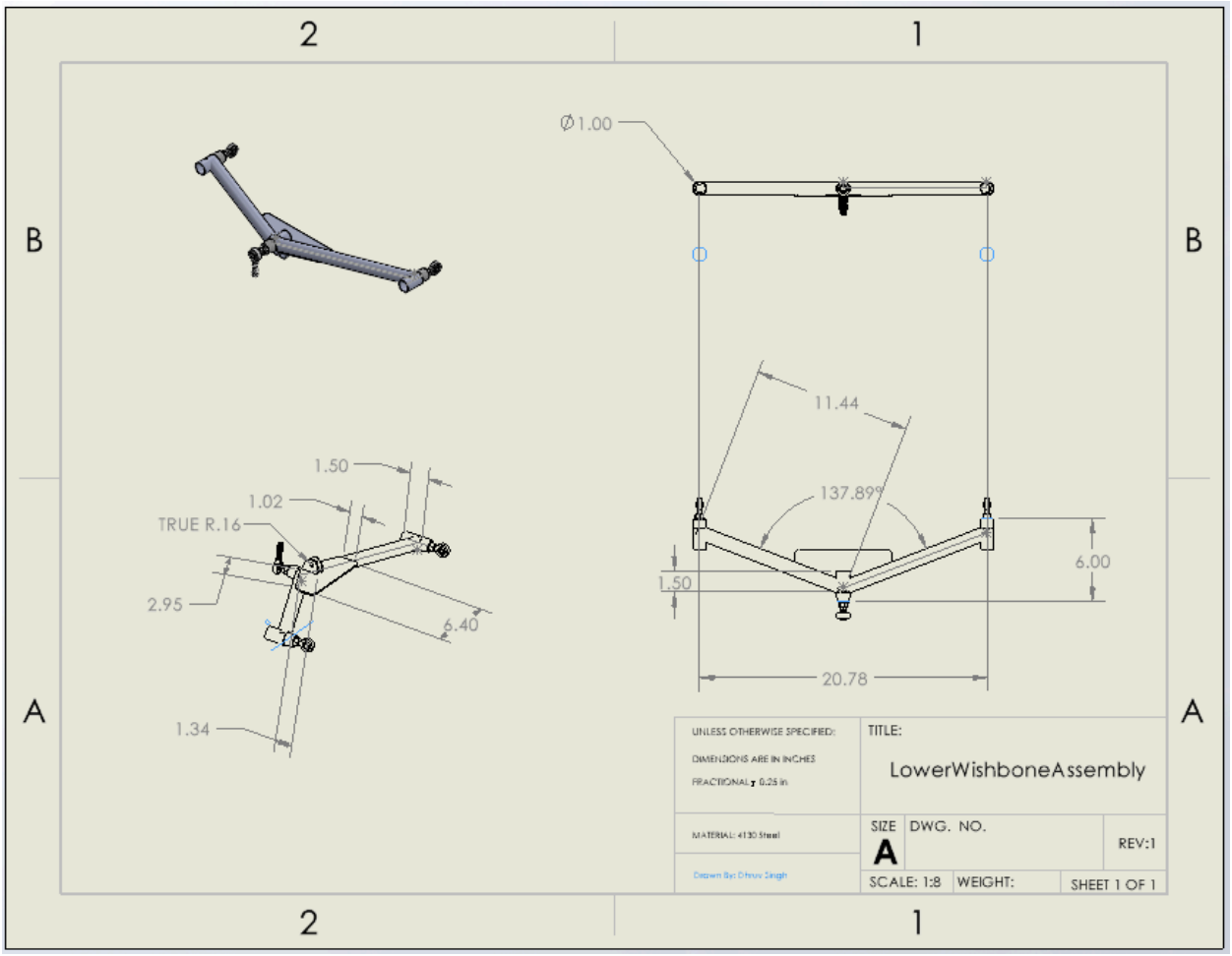

Figure C.3: Lower Wishbone Assembly Drawing

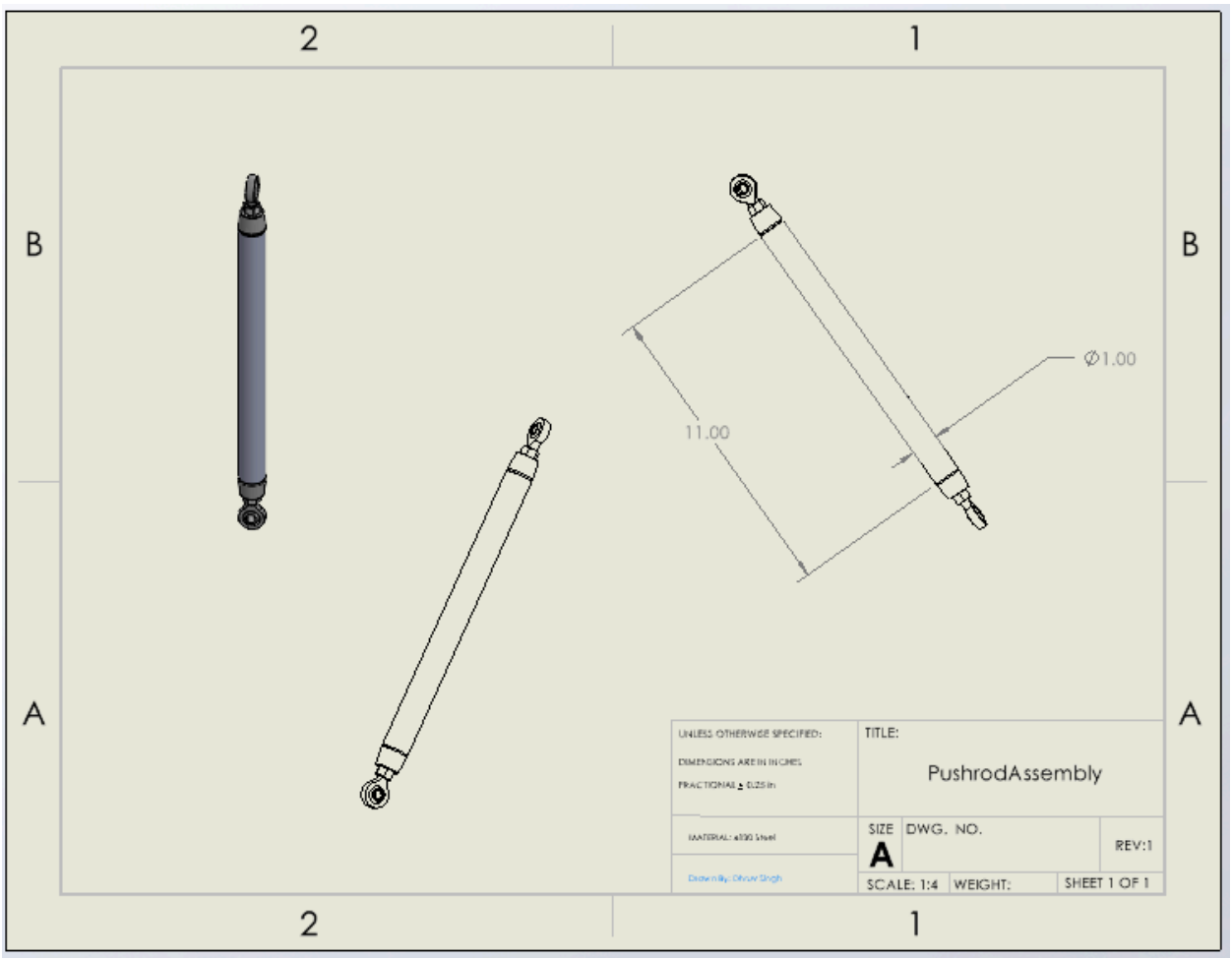

Figure C.4: Pushrod Assembly Drawing

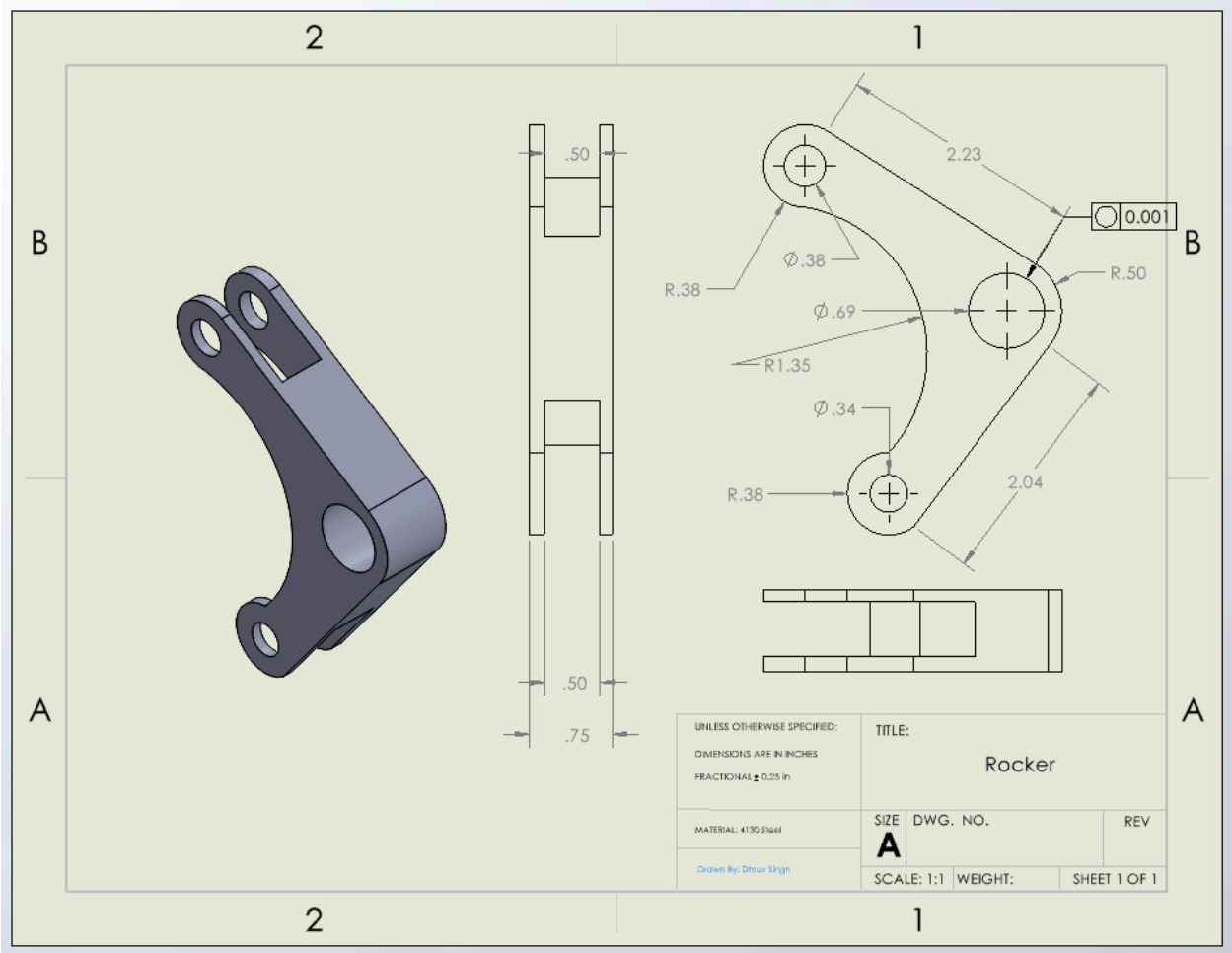

Figure C.5: Rocker Drawing

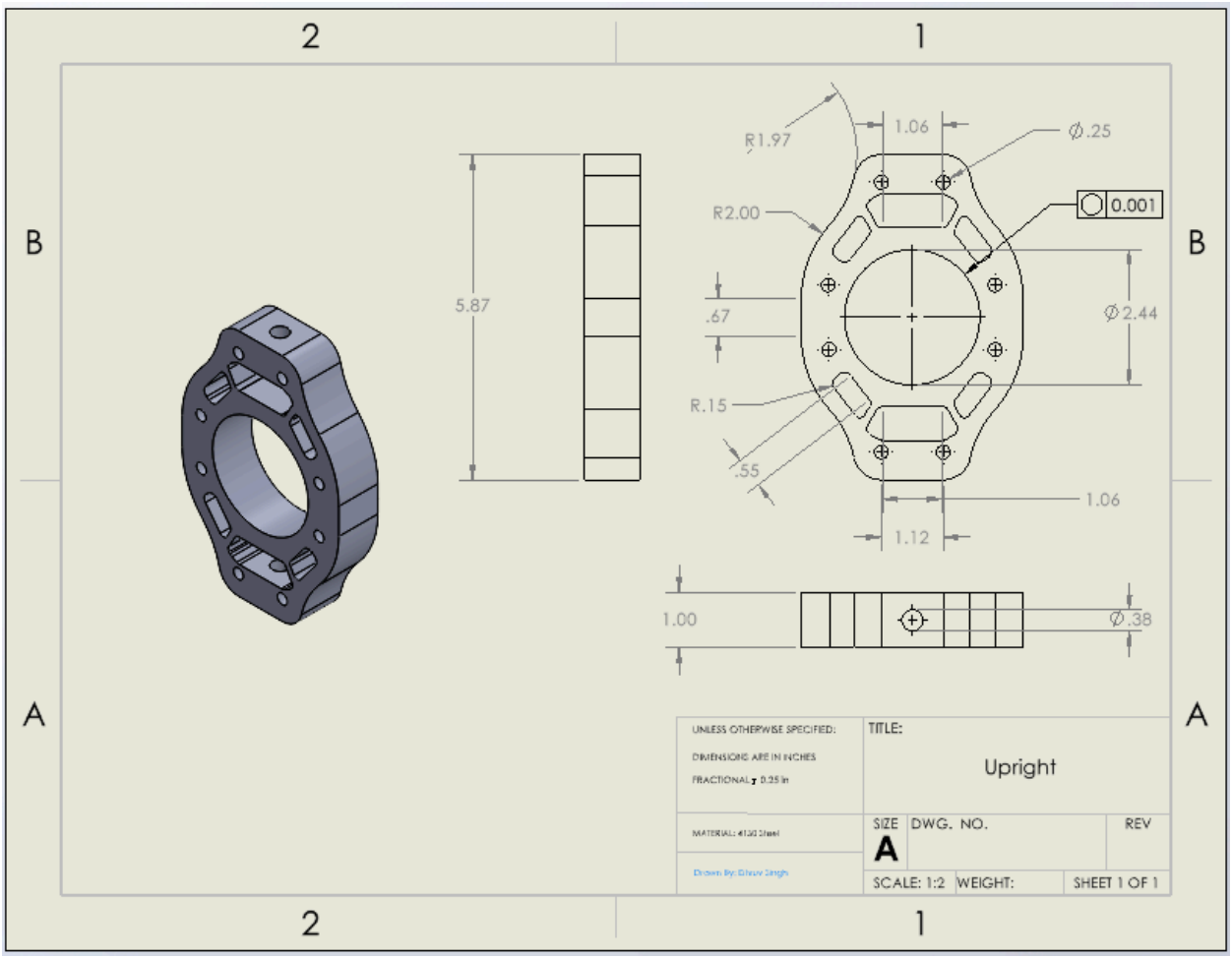

Figure C.6: Upright Drawing

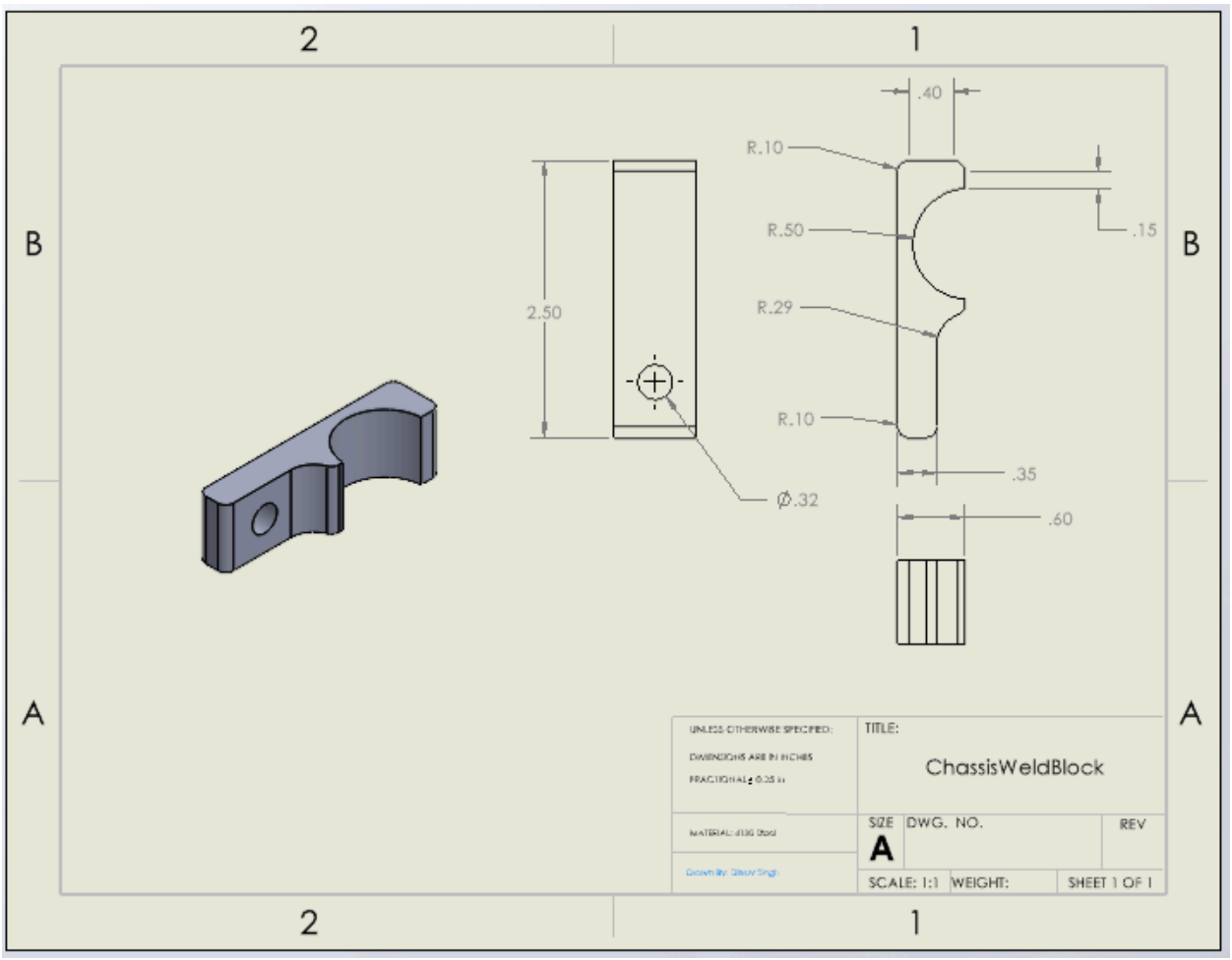

Figure C.7: Chassis Weld Block Drawing

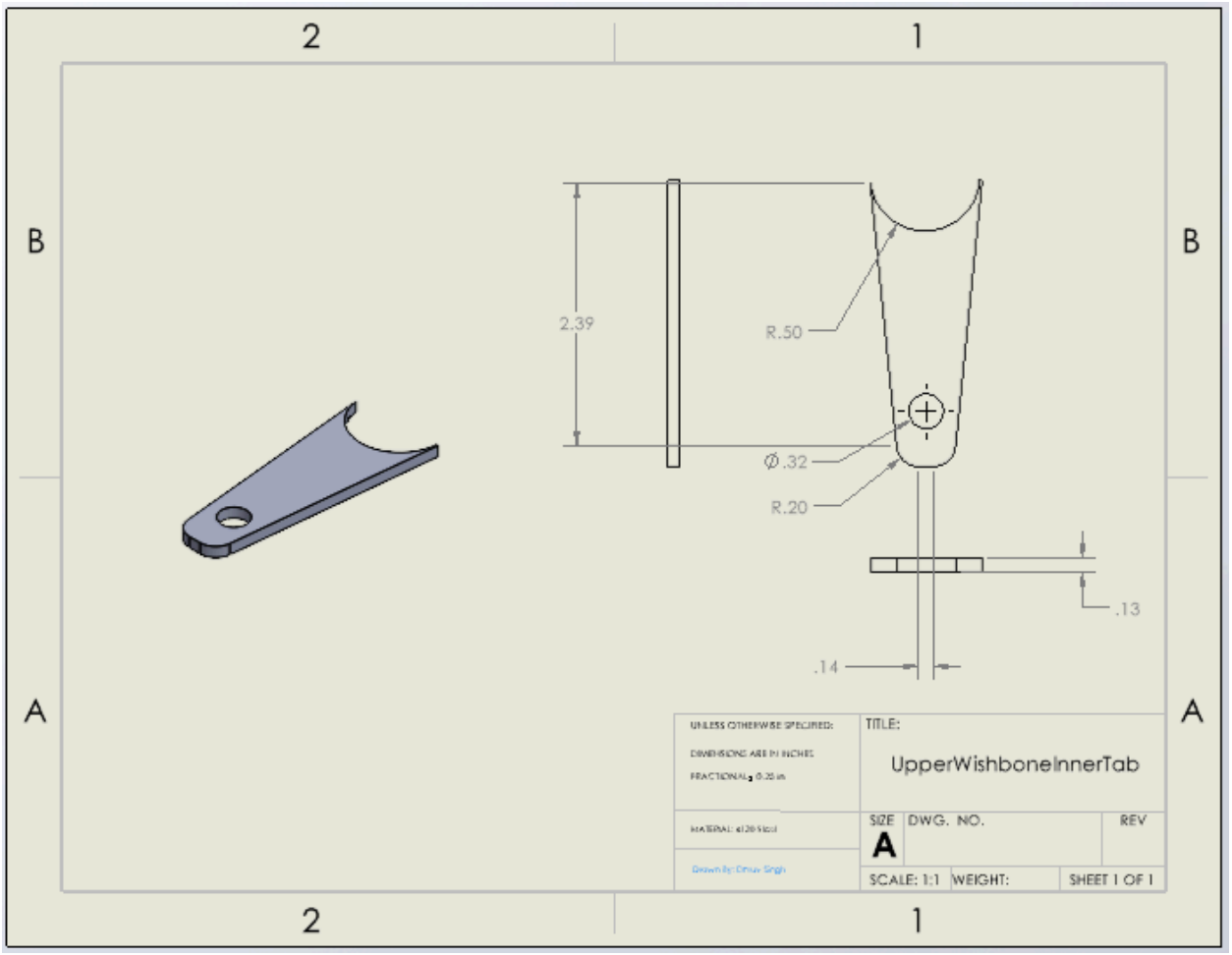

Figure C.8: Upper Wishbone Inner Tab Drawing

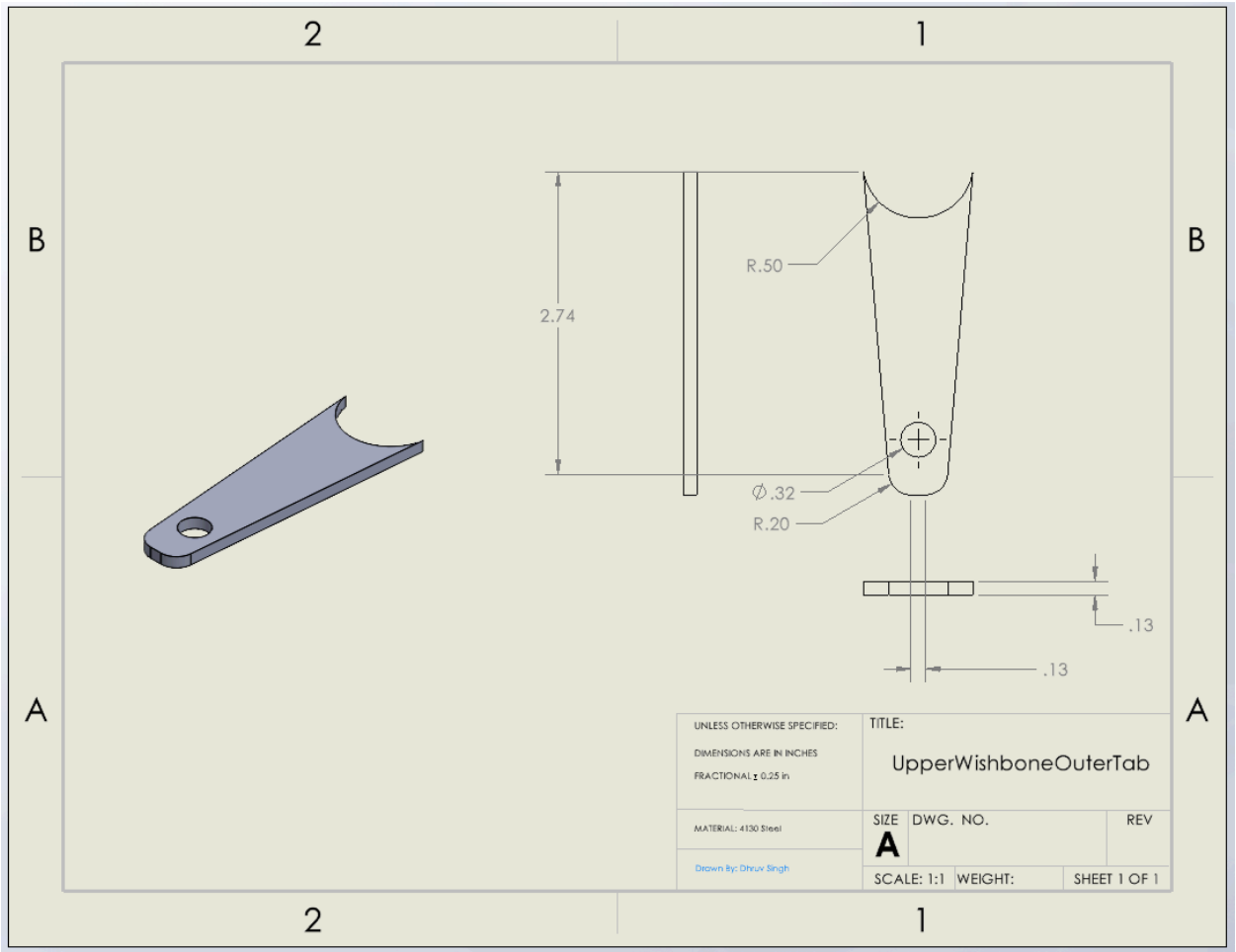

Figure C.9: Upper Wishbone Outer Tab Drawing

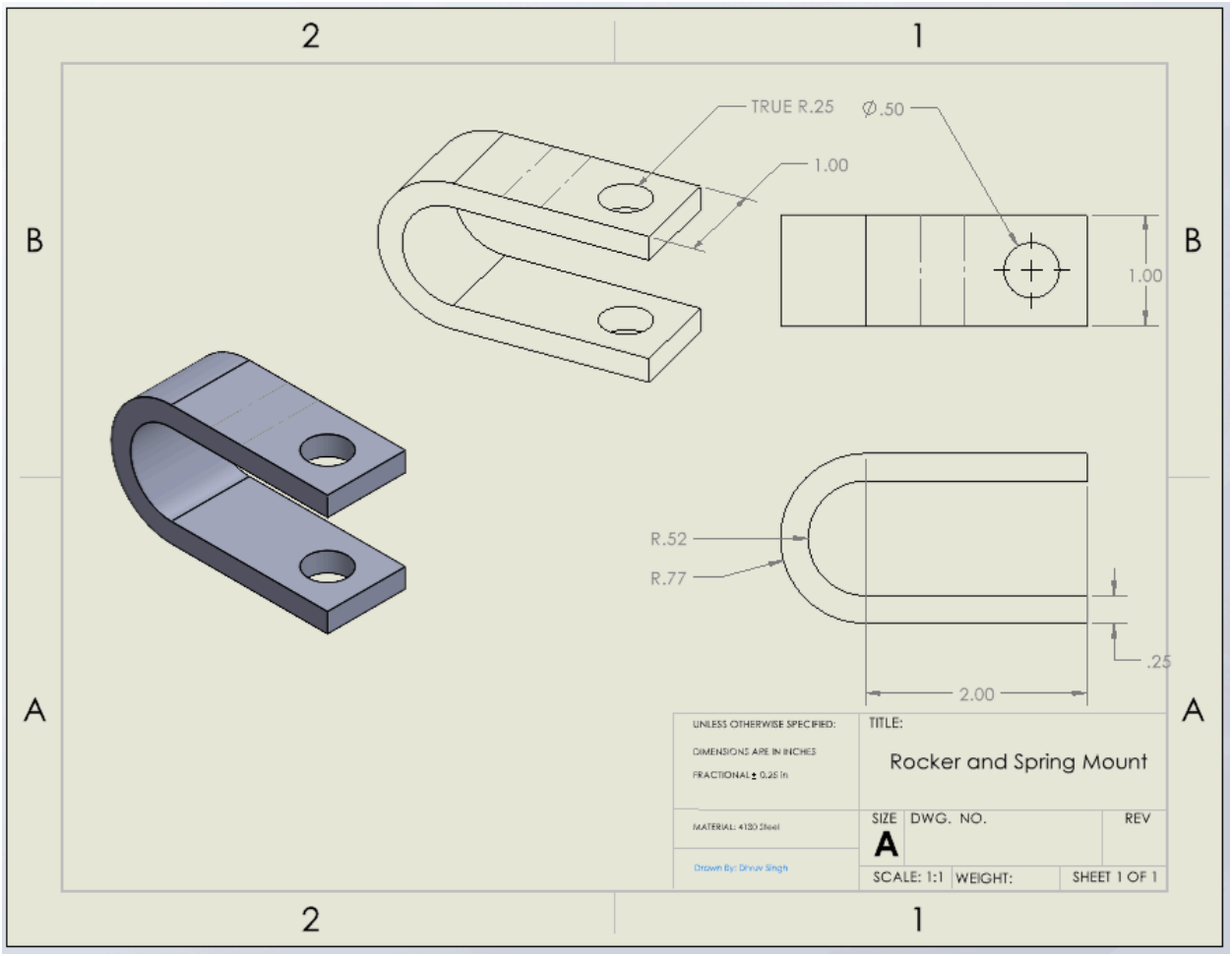

Figure C.10: Rocker and Spring Mount Drawing

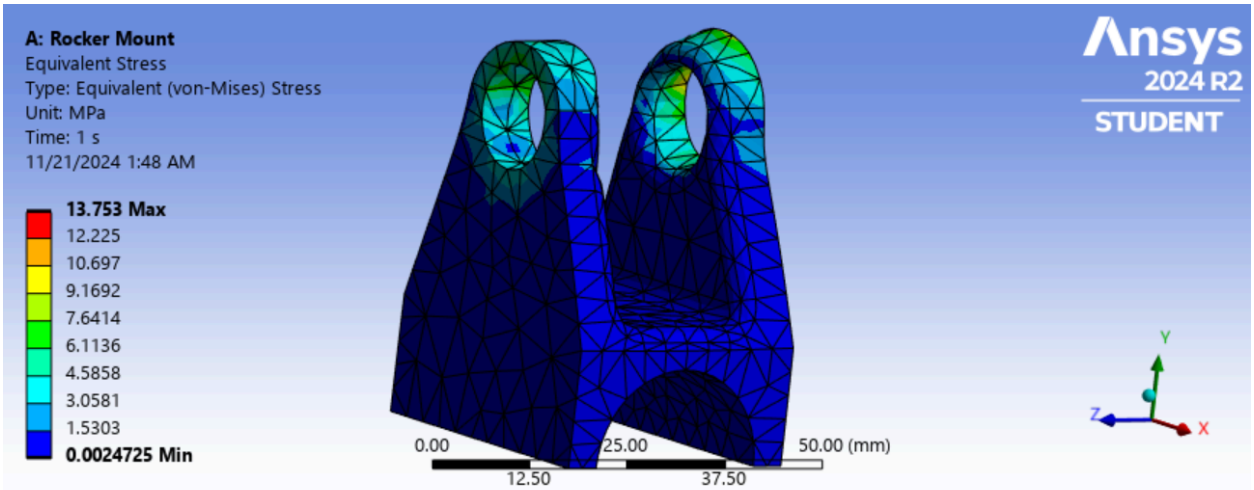

Figure C.11. Finite Element Analysis Stress Map of Rocker Mount

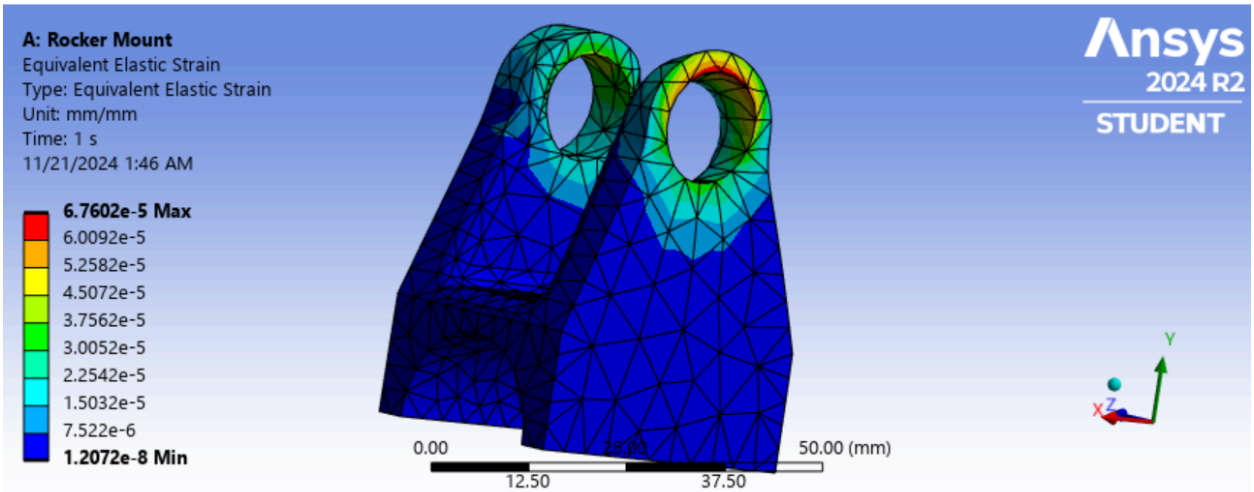

Figure C.12. Finite Element Analysis Strain Map of Rocker Mount

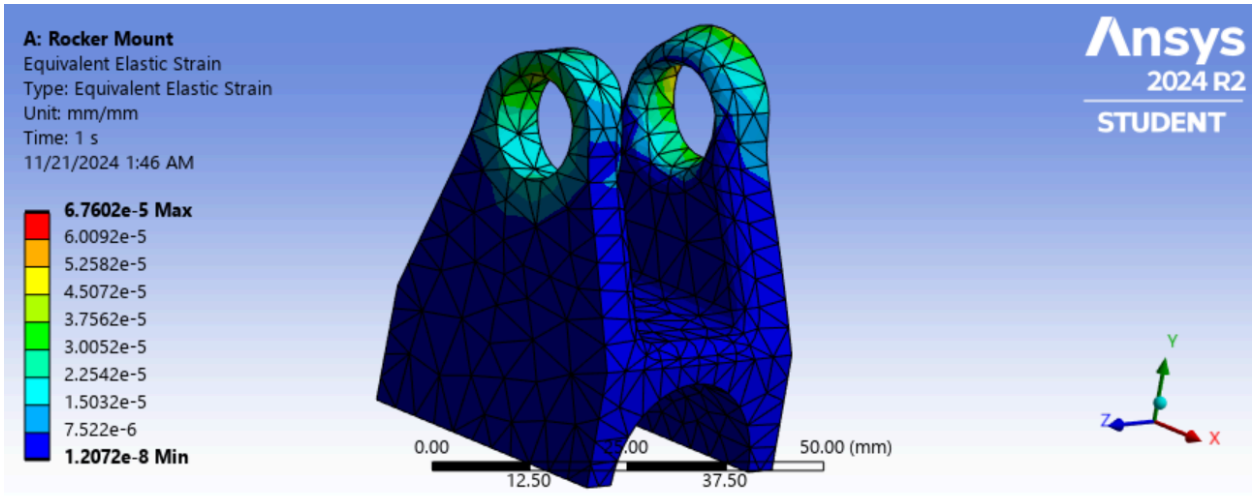

Figure C.13. Finite Element Analysis Strain Map of Rocker Mount

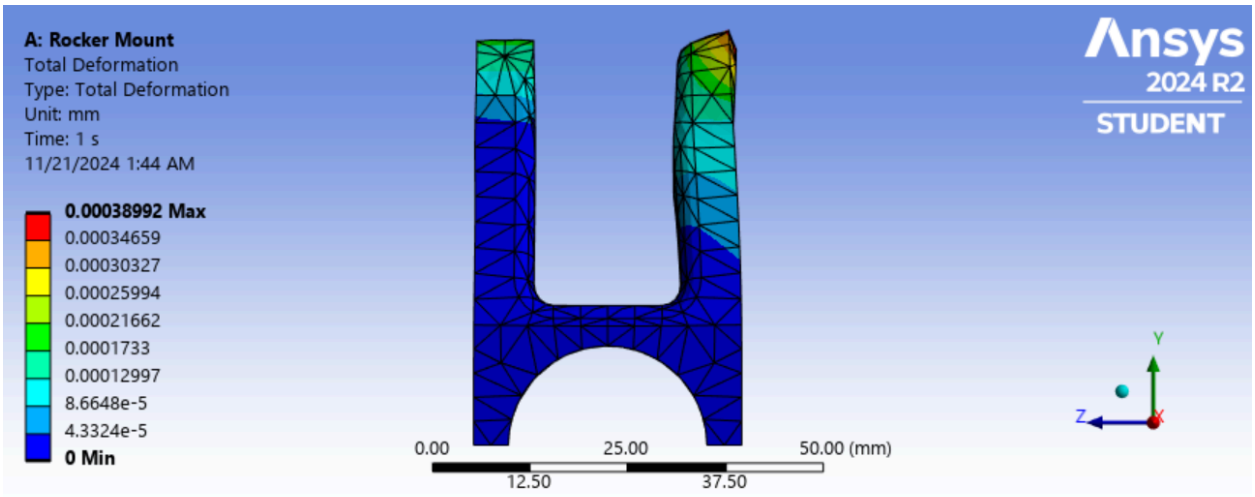

Figure C.14. Finite Element Analysis Deformation Map of Rocker Mount

Analysis Objective:

The objective of the FEA was to evaluate the **structural performance** of the "Rocker Mount" under loading conditions. Specifically, the analysis focused on:

- ➔ Equivalent (von-Mises) Stress distribution.
- ➔ Equivalent Elastic Strain distribution.

Material and Loading:

- ➔ The material used for the analysis was likely isotropic, with properties set in ANSYS.
- ➔ The loads applied are unspecified in the images but are concentrated in areas influencing the stress and strain around the mounting holes.

Results:

Equivalent von-Mises Stress

1. **Peak Stress**: The maximum equivalent stress is approximately **13.753 MPa**, occurring around the upper region near the mounting holes.
2. **Stress Distribution:**

- ➔ The highest stress regions are located at the contact areas and edges of the mounting holes.
- ➔ Stress decreases progressively toward the base and outer surfaces, as shown in the color gradient.

3. **Minimum Stress**: Near **0.0024725 MPa**, observed in areas farther from load application.

Equivalent Elastic Strain:

1. **Peak Strain**: The maximum elastic strain observed is approximately **6.7602e-5 mm/mm**, concentrated around the mounting holes, coinciding with high-stress areas.
2. **Strain Distribution**:

- ➔ Strain is localized near the mounting holes, indicating deformation is most significant in these regions.
- ➔ Lower strain values are seen across the bulk of the structure, showing limited deformation.

Mesh Information:

- ➔ The model uses a tetrahedral mesh with refined elements around high-stress regions (e.g., holes) to improve accuracy.
- ➔ Uniform mesh quality is maintained elsewhere.

Interpretation:

1. **Structural Integrity:**
    - ➔ The stress values are within typical limits for most metals and polymers (depending on the material used).
    - ➔ High-stress concentration around the holes suggests a potential for localized failure under higher loads.
2. **Elastic Deformation:**
    - ➔ The strain values indicate minor deformation, suggesting the structure is likely operating in the elastic regime under the applied load.

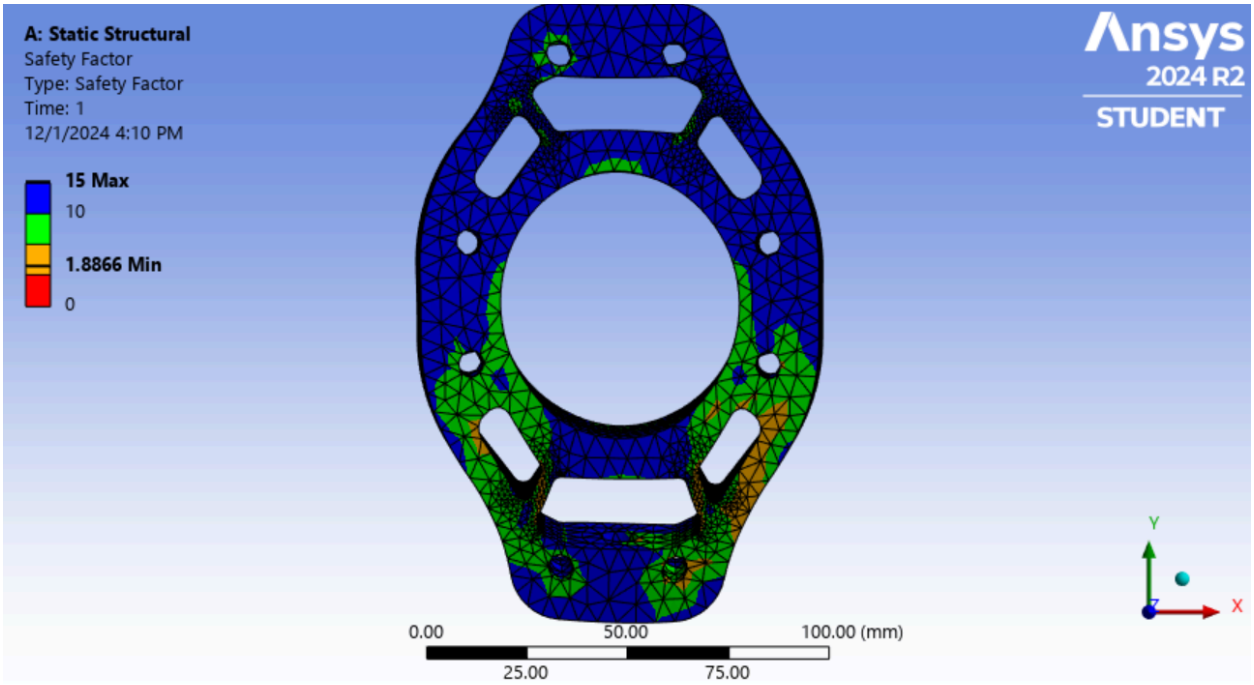

Figure C.15. Finite Element Analysis Safety Factor Map of Upright Braking

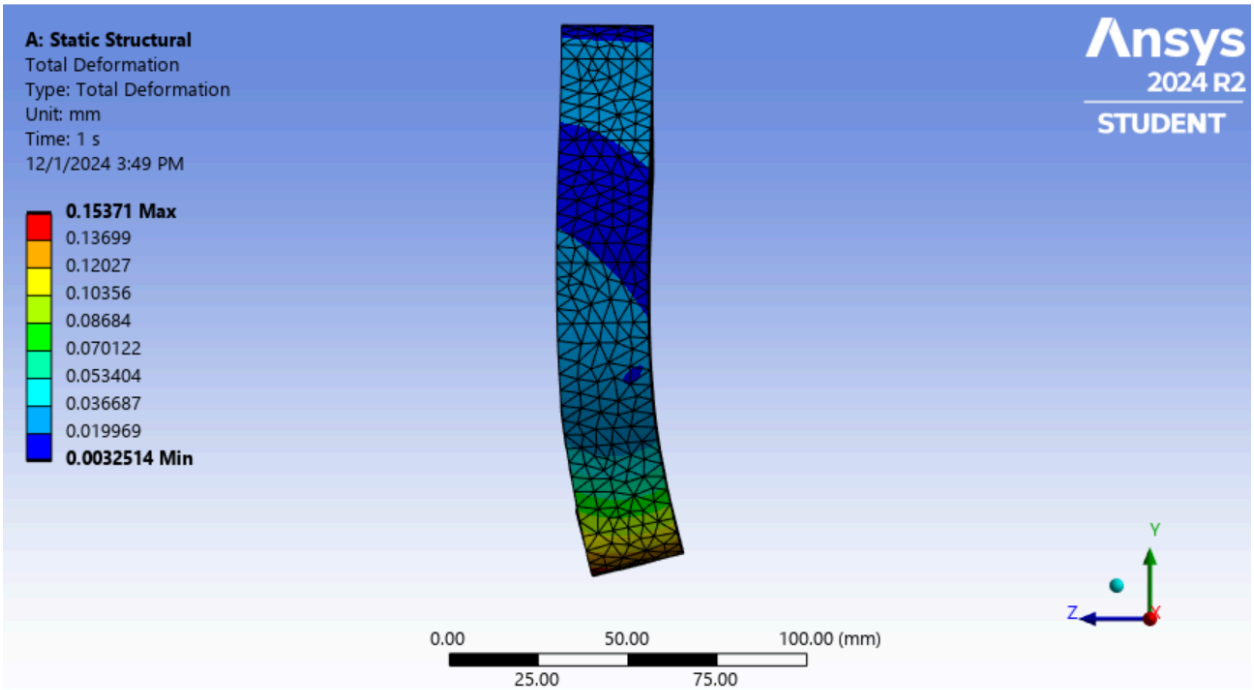

Figure C.16. Finite Element Analysis Deformation Map of Upright Braking

Analysis Objective:

The purpose of this analysis is to evaluate the **mechanical performance** of the "Upright" under static structural loading. Key aspects analyzed include:

- ➔ Total deformation
- ➔ Von-Mises stress distribution
- ➔ Equivalent elastic strain
- ➔ Safety factor distribution

Applied Loads and Constraints:

1. **Loads:**

➔ **Bearing Load (A):** 8006.8 N, applied at a specific bearing interface.
➔ **Remote Forces (B and E):** 2001.7 N (horizontal) and 4716.2 N (diagonal).
➔ **Remote Displacement (C):** A constraint limiting deformation.

2. **Supports:**

➔ **Cylindrical Support (D):** Fixed to prevent translation and rotation.

Results Overview:

1. Total Deformation:

➔ **Maximum Deformation:** ~0.15371 mm
- Located at the top regions of the upright structure, furthest from the constrained areas.

➔ **Minimum Deformation:** ~0.0032514 mm
- Found near the fixed support regions.

2. Von-Mises Stress Distribution:

- **Maximum Stress:** 155.56 MPa
    - Observed around sharp edges and near applied load areas, such as hole edges.
- **Minimum Stress:** ~0.28856 MPa
    - Spread over the bulk of the structure, away from load concentrations.
- **Stress Interpretation:** The upright is subjected to high-stress concentrations around connection points and loading regions. This suggests areas of potential structural optimization.

3. Equivalent Elastic Strain

➔ **Maximum Strain:** 0.0022573 mm/mm
- Found near the high-stress regions around the holes and edges.

➔ **Minimum Strain:** 5.4033e-6 mm/mm
- Located away from stress concentration points, within the bulk of the structure.

➔ **Elastic Behavior:** Strain levels indicate that the material is within its elastic range, assuming the yield strain exceeds the maximum observed strain.

4. Safety Factor:

➔ **Minimum Safety Factor:** 1.6214

- Occurs in regions of high stress around sharp edges and load application points.

➔ **Maximum Safety Factor:** 15

- Found in areas with minimal stress and strain.

➔ **Interpretation:** The safety factor analysis indicates localized vulnerabilities near stress concentration areas. A factor above 1 ensures that the material can withstand the applied loads but may require design improvements for areas near the lower safety factor threshold.

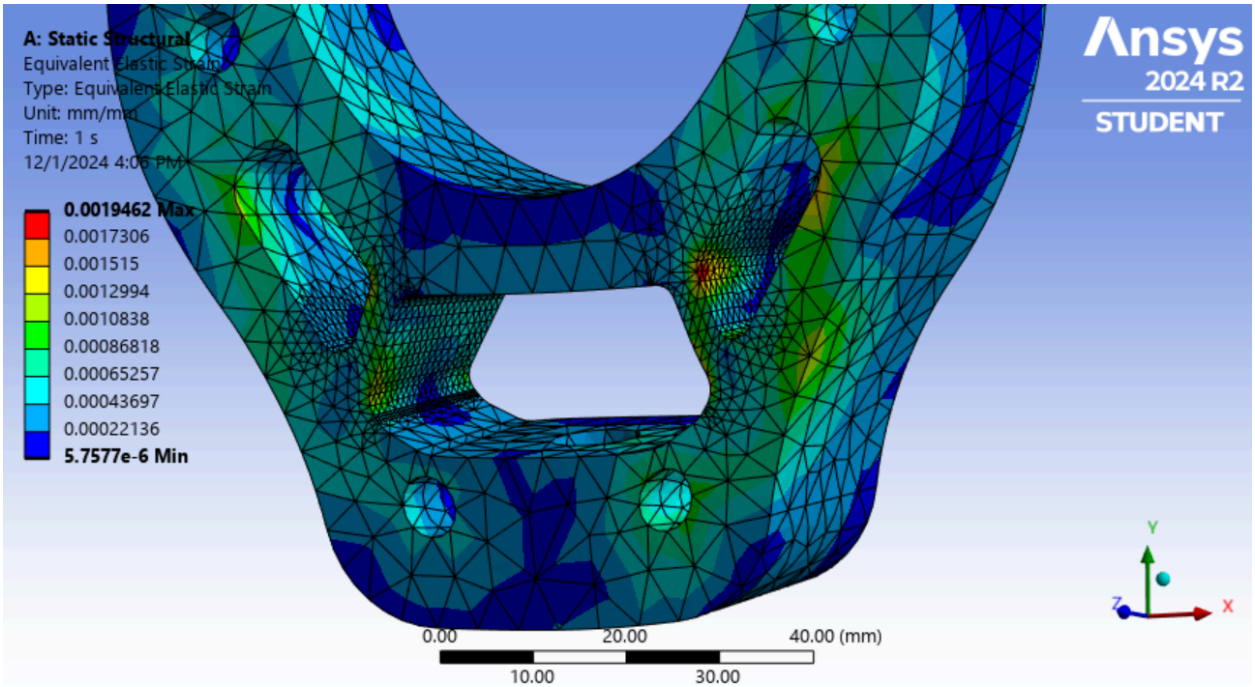

Figure C.17: FEA Strain Map of Upright Braking

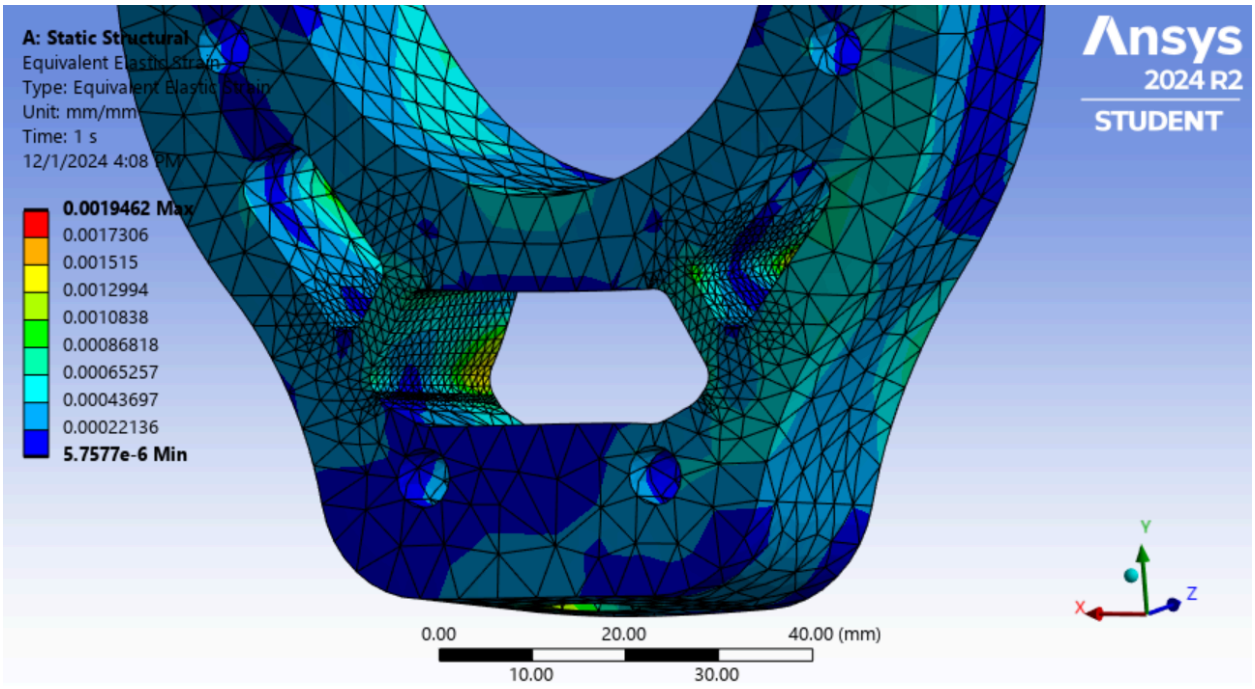

Figure C.18: FEA Strain Map of Upright Braking

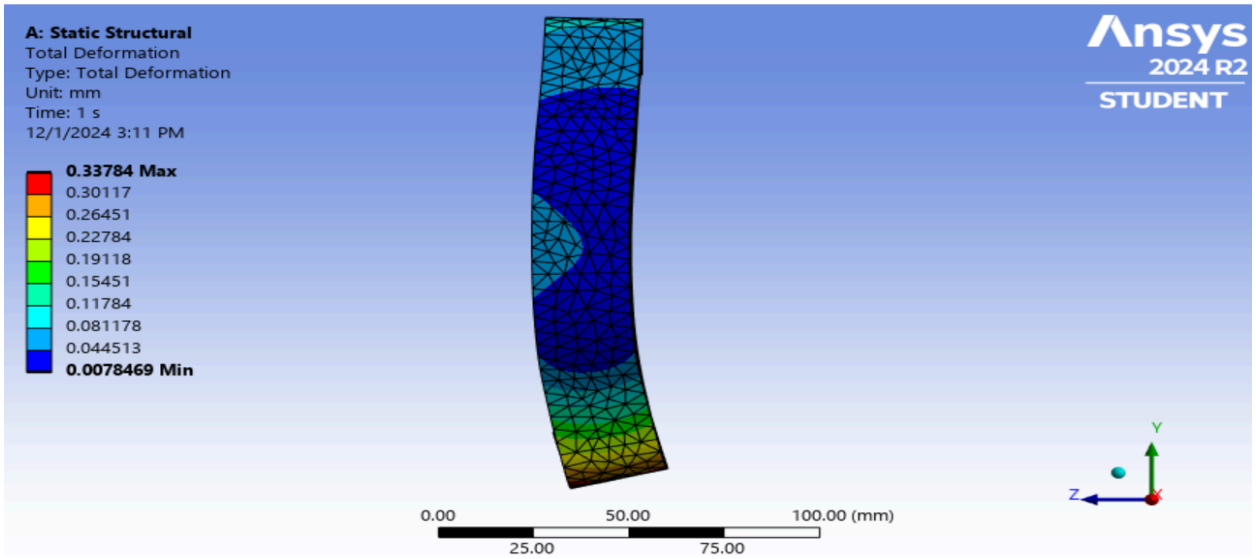

Figure C.19: FEA Deformation Map of Upright Braking

Analysis Objective:

The objective of this Finite Element Analysis (FEA) is to evaluate the structural integrity of the upright under applied static loads and constraints. The study assesses:

- Total deformation.
- Equivalent stress (von-Mises stress).
- Equivalent elastic strain.
- Safety factor distribution.

Applied Loads and Constraints:

1. **Loads:**

➔ **Bearing Load (A):** 8006.8 N applied vertically.
➔ **Remote Forces (B and E):** 2001.7 N (horizontal) and 4716.2 N (diagonal).
➔ **Remote Displacement (C):** Applied to constrain specific degrees of freedom.

2. **Supports:**

➔ **Cylindrical Support (D):** Fully fixed, preventing translation and rotation in all axes.

Results Summary

1. Total Deformation

- **Maximum Deformation:** 0.33784 mm

➔ Located at the regions farthest from the fixed constraints, primarily near the vertical extent of the upright.

- **Minimum Deformation:** 0.0078469 mm

➔ Found near the support and loading regions.

- **Deformation Interpretation:** Deformation remains minimal, indicating that the structure is relatively stiff under the applied loading conditions.

2. Equivalent von-Mises Stress

- **Maximum Stress:** 134.13 MPa

➔ Occurs around sharp edges near the loading areas, especially near the bolt holes.

- **Minimum Stress:** 0.27881 MPa

➔ Spread across the less critical sections of the upright, far from stress concentration zones.

- **Stress Interpretation:** The stress distribution highlights areas susceptible to stress concentration, which may require reinforcement or design modifications.

3. Equivalent Elastic Strain

- **Maximum Strain:** 0.0019462 mm/mm

➔ Found near the same high-stress regions around the mounting holes.

- **Minimum Strain:** 5.7577e-6 mm/mm

➔ Distributed across the body of the upright in low-stress regions.

- **Strain Interpretation:** The elastic strain values confirm that the material operates in its elastic range under the given loading conditions.

4. Safety Factor

- **Minimum Safety Factor:** Not explicitly shown in the provided images, but inferred to be above 1.
- **Safety Factor Interpretation:** Regions with lower safety factors align with the high-stress and high-strain areas. While the upright maintains structural integrity, these areas should be reviewed for potential improvements.

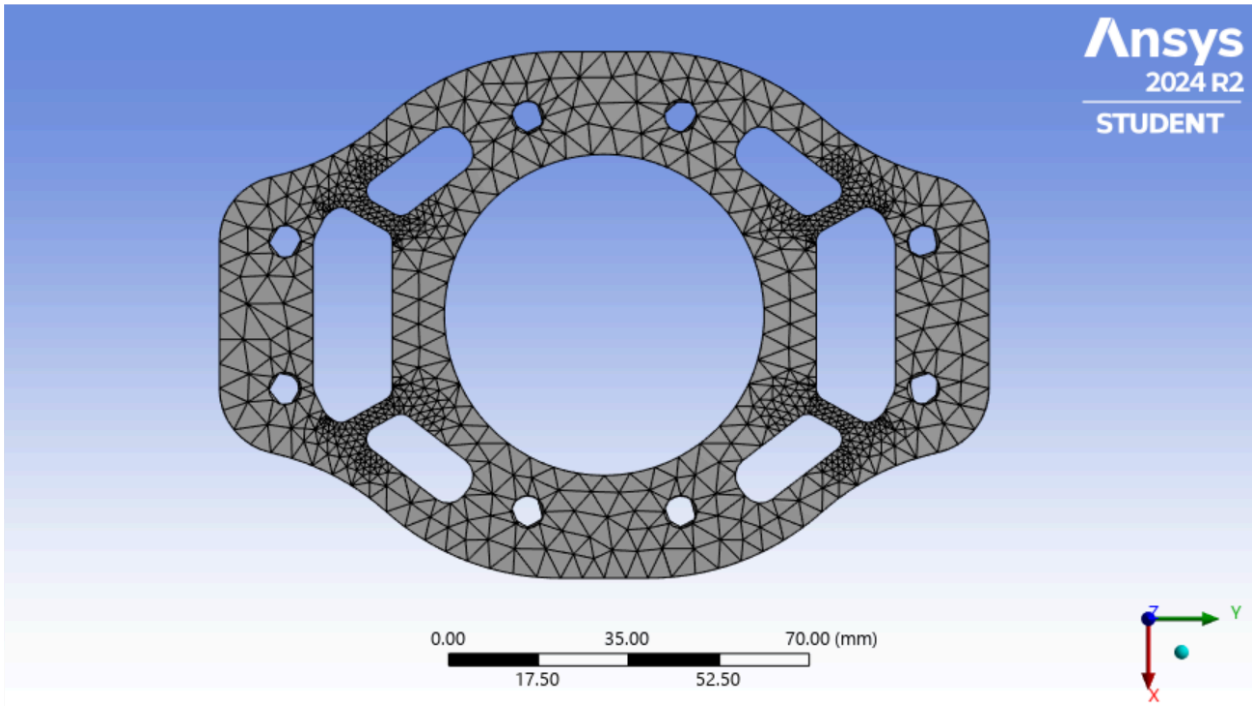

Figure C.20: Upright Cornering FEA

Analysis Objective:

The analysis aims to evaluate the **mechanical behavior** of the upright component under applied loads and constraints. The study investigates:

- Total deformation
- Von-Mises stress distribution
- Equivalent elastic strain
- Safety factor distribution
- Mesh quality

Applied Loads and Constraints:

1. **Loads:**
- **Bearing Load (A):** 8006.8 N applied vertically.
- **Remote Forces (B and E):** 4003.4 N (horizontal) and 5568.3 N (diagonal).
- **Remote Displacement (C):** Applied to limit movement along specific axes.
2. **Supports:**
- **Cylindrical Support (D):** Fully fixed to prevent translation and rotation in all axes.

Results Summary

1. Total Deformation

- **Maximum Deformation:** 0.33784 mm
  ➔ Occurs in the free sections farthest from the fixed constraints, such as the outer edges of the component.
- **Minimum Deformation:** 0.0078469 mm
  ➔ Located near the fixed support regions, where movement is restricted.
- **Interpretation:** The deformation is minimal, confirming the component's structural stiffness under the applied loads.

2. Von-Mises Stress

- **Maximum Stress:** 254.67 MPa
  ➔ Concentrated around sharp edges and holes where loads are applied.
- **Minimum Stress:** 0.98663 MPa
  ➔ Found across the less stressed regions, away from load concentrations.

- **Interpretation:** High-stress regions indicate potential failure zones, especially near connection points and edges.

3. Equivalent Elastic Strain

- **Maximum Strain:** 0.0036991 mm/mm
  ➔ Observed near high-stress regions around the holes and sharp edges.
- **Minimum Strain:** 2.2836e-5 mm/mm
  ➔ Spread throughout the bulk material in low-stress areas.
- **Interpretation:** The elastic strain values confirm the material remains within its elastic range, assuming a yield strain above the maximum observed strain.

4. Safety Factor

- **Minimum Safety Factor:** 1.0074
  ➔ Found in the high-stress zones, indicating these regions are near the material's yield limit.
- **Maximum Safety Factor:** 15
  ➔ Found in low-stress areas, demonstrating high safety margins.
- **Interpretation:** The component is structurally sound but exhibits critical zones where the safety factor is low, requiring design improvements.

5. Mesh Quality

- **Mesh Distribution:** A fine mesh is used around high-stress regions (e.g., edges and holes) to ensure accurate results.
- **Global Mesh Quality:** Uniformly distributed with no major irregularities, suitable for the analysis.

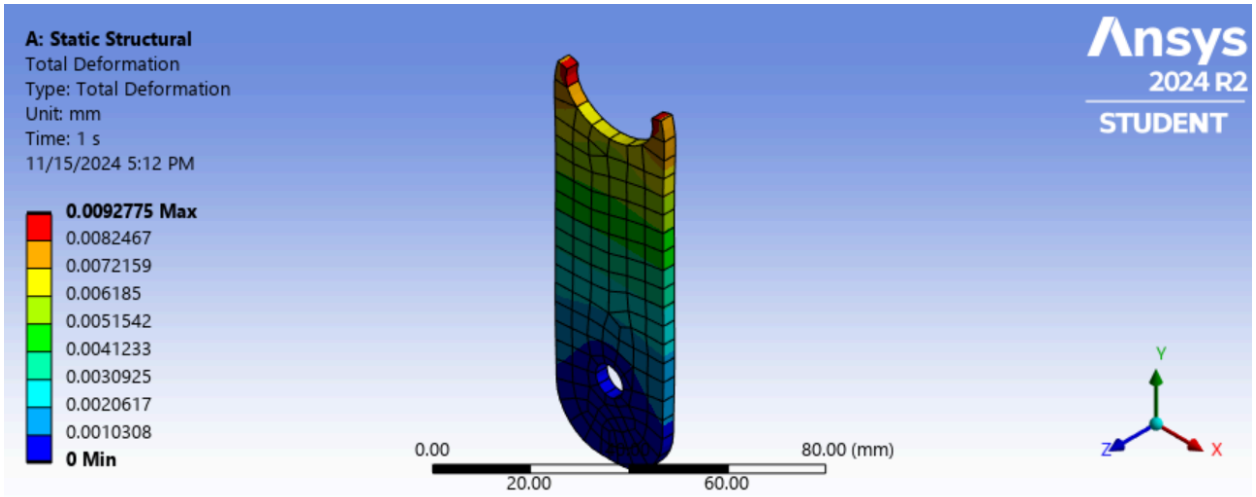

Figure C.21. Finite Element Analysis of Weld Tab

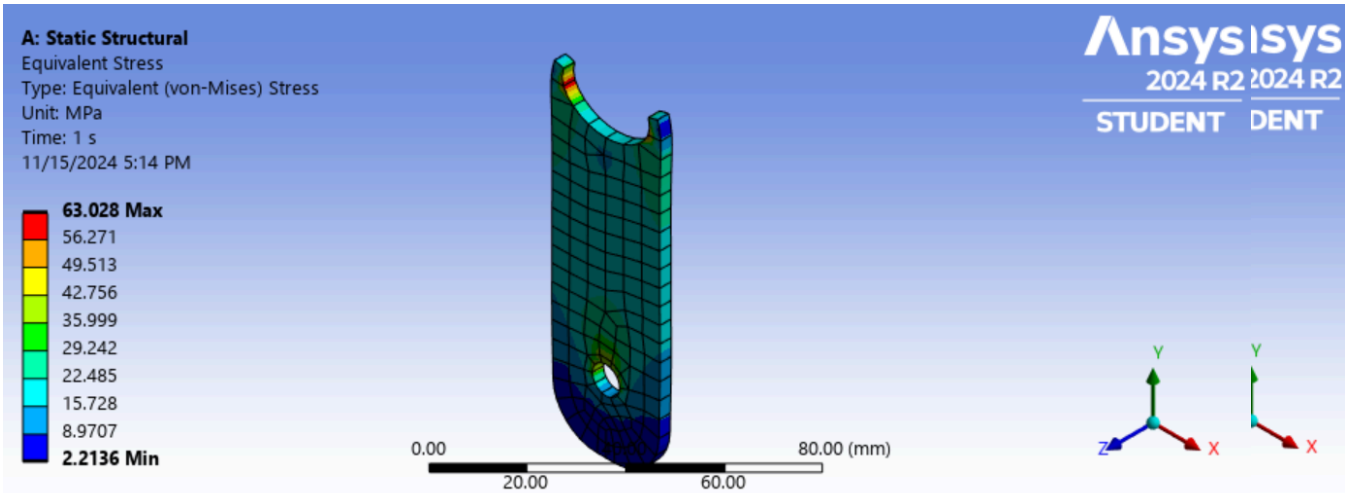

Figure C.22. Finite Element Analysis of Weld Tab

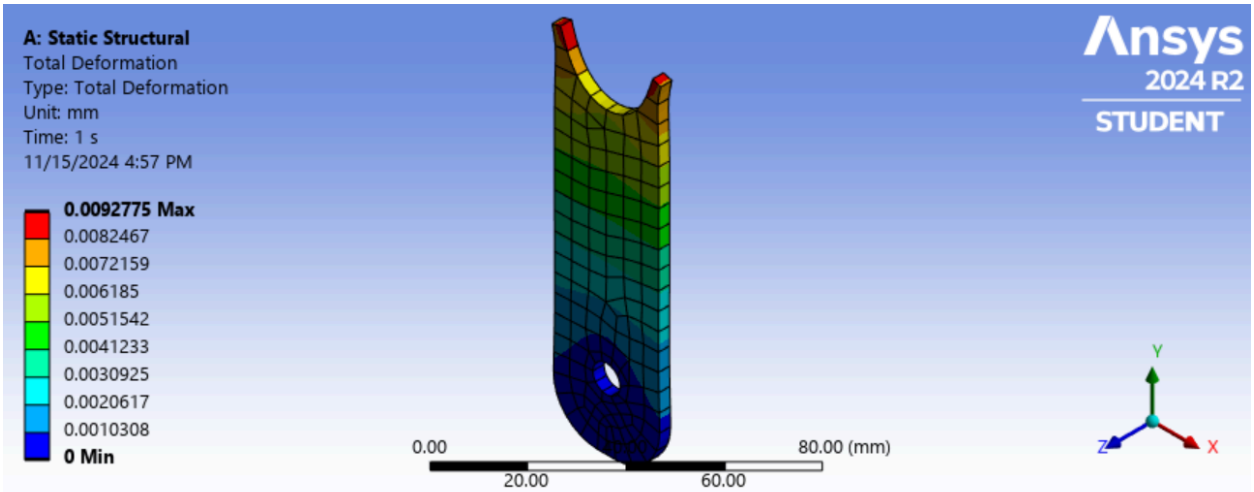

Figure C.23: *Finite Element Analysis of Weld Tab*

Analysis Objective:

The purpose of this FEA is to evaluate the structural response of the component under an applied load and fixed support. The analysis aims to determine:

- Total deformation.
- Equivalent von-Mises stress.
- Equivalent elastic strain.

Applied Loads and Constraints:

1. **Loads:**

➔ **Force (A):** 1957.2 N applied at the curved top surface.

2. **Supports:**

➔ **Fixed Support (B):** Constrained at the bottom hole, preventing any translation or rotation.

Results Summary:

1. Total Deformation

- **Maximum Deformation:** 0.0092775 mm

➔ Occurs at the topmost portion where the load is applied, farthest from the fixed support.

- **Minimum Deformation:** 0 mm

➔ Found at the fixed support location.

- **Interpretation:** The deformation is minimal, suggesting the component is stiff and resistant to displacement under the applied load.

2. Equivalent von-Mises Stress

- **Maximum Stress:** 63.028 MPa

➔ Concentrated at the intersection between the curved top and the vertical flat section, as well as around the hole near the fixed support.

- **Minimum Stress:** 2.2136 MPa

➔ Distributed in the bulk of the component, away from critical points.

- **Interpretation:** The stress distribution indicates areas where failure may initiate under higher loads. The maximum stress is likely within the material's yield limit, assuming a material with sufficient strength.

3. Equivalent Elastic Strain

- **Maximum Strain:** 0.00030832 mm/mm

➔ Observed near high-stress regions at the curved top and hole area.

- **Minimum Strain:** 1.796e-5 mm/mm

➔ Found in regions experiencing minimal deformation and stress.

- **Interpretation:** The low strain values suggest that the part is operating in the elastic region, assuming a material with adequate yield strain.

Mesh Details

- A structured mesh with finer elements in regions near the load application and fixed support, ensuring accurate stress and strain predictions in critical areas.

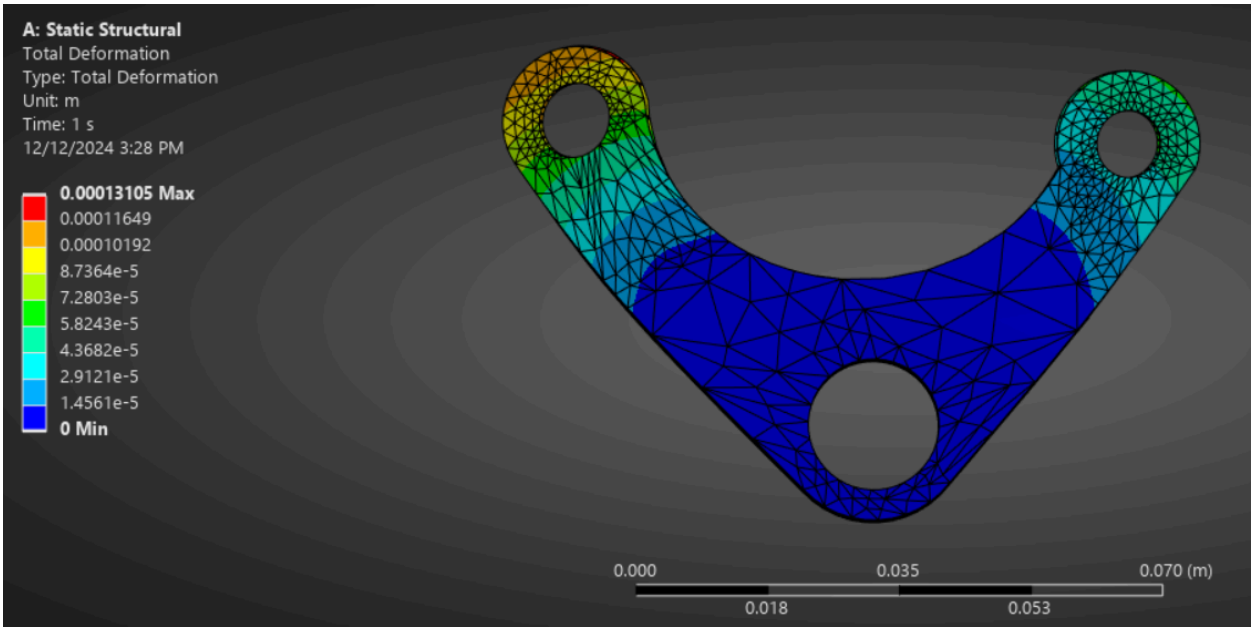

Figure C.24: Finite Element Analysis of Rocker

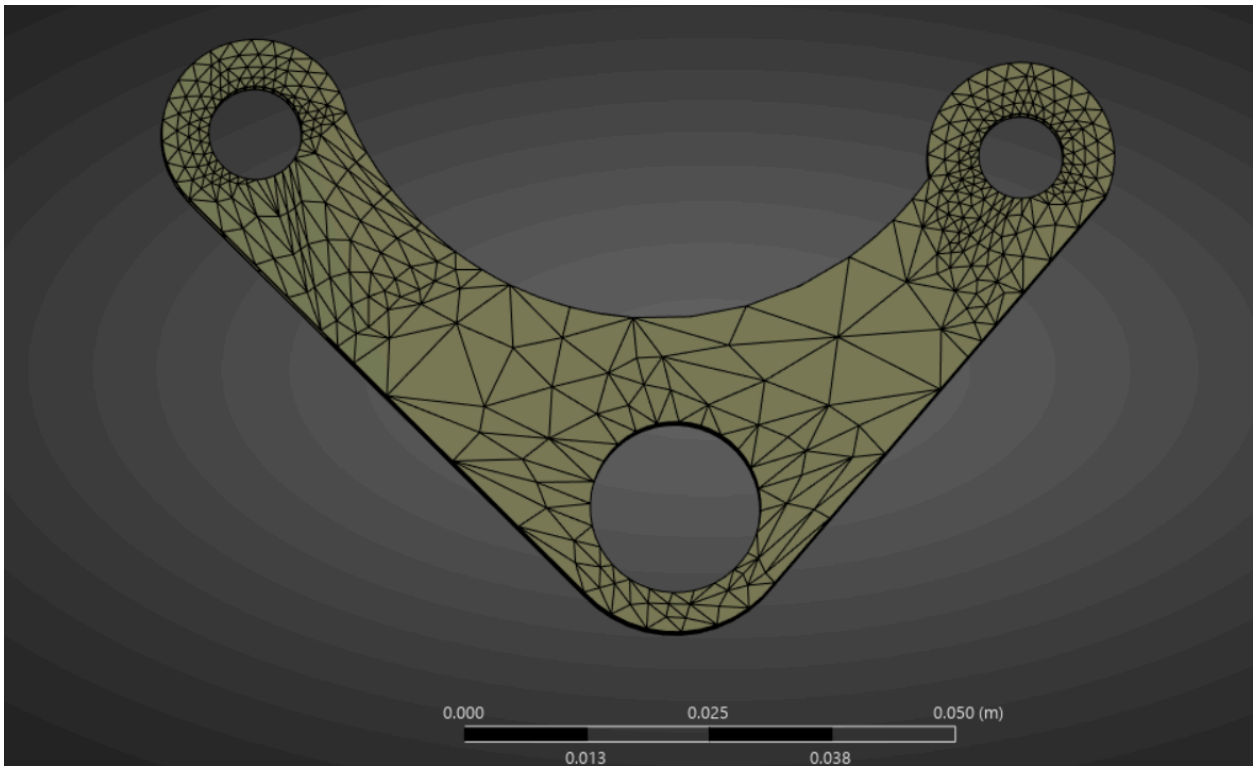

Figure C.25: Finite Element Analysis of Rocker

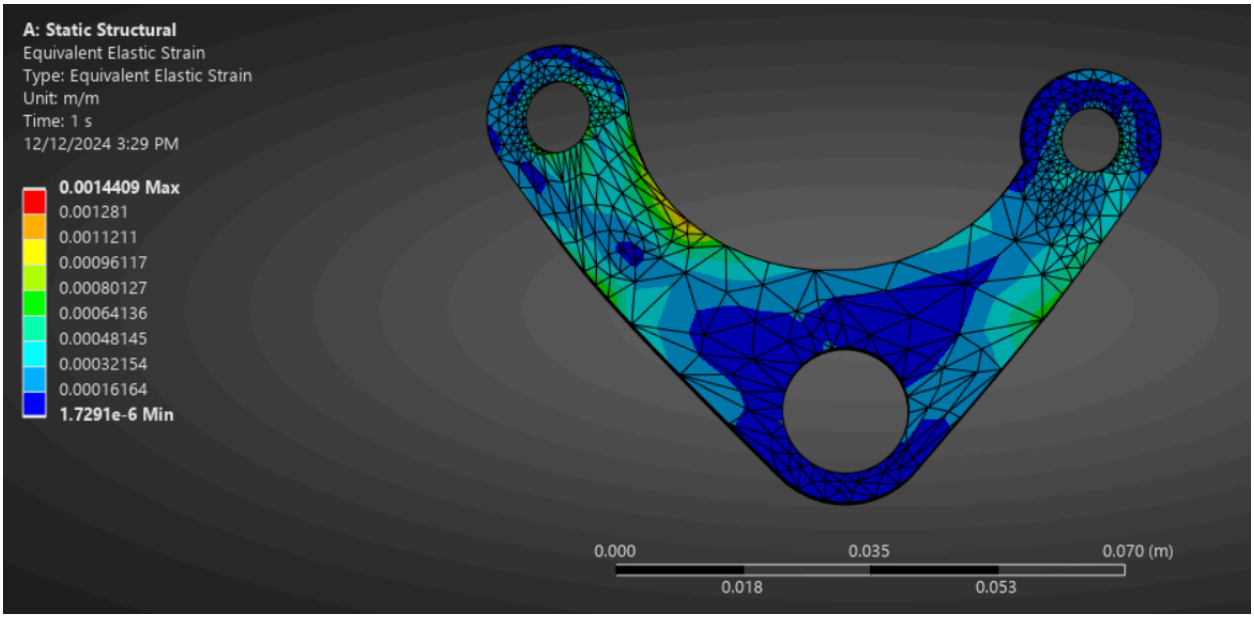

Figure C.26: Finite Element Analysis of Rocker

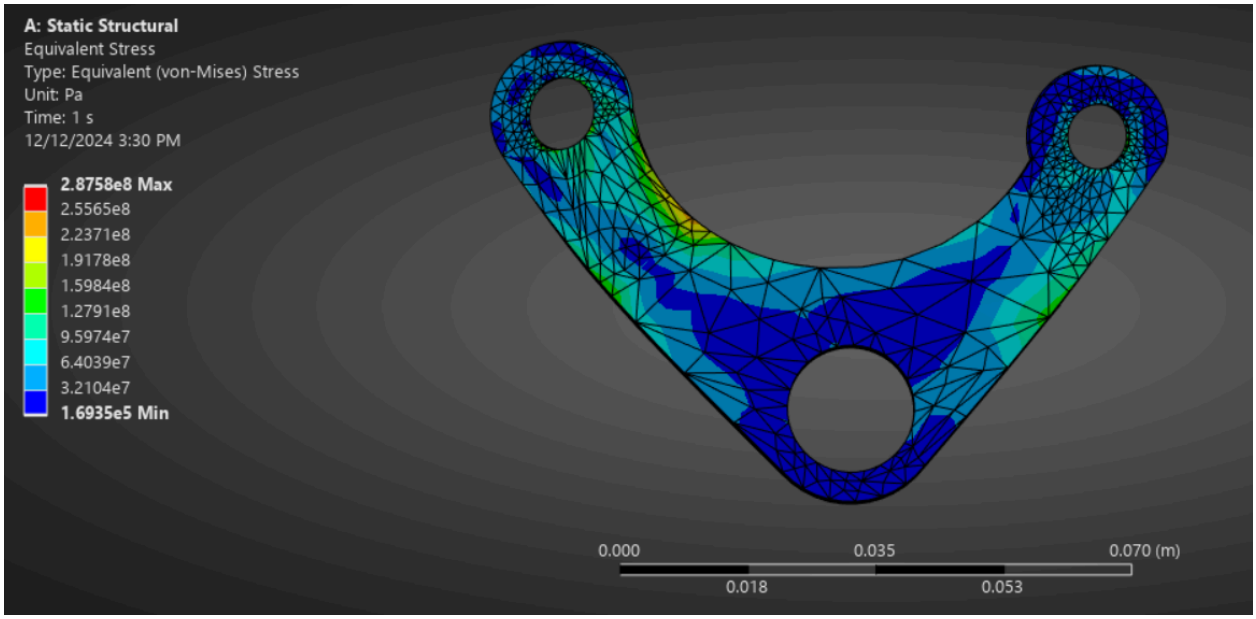

Figure C.27: Finite Element Analysis of Rocker

Analysis Objective

The purpose of this analysis is to evaluate the mechanical behavior of the component under static loading. The study examines:

- Total deformation
- Equivalent von-Mises stress
- Equivalent elastic strain
- Load and boundary conditions
- Mesh quality

Applied Loads and Constraints

1. **Loads:**

➔ **Remote Forces (A, B, C, D):** Four forces of 2136.9 N each applied at the top two holes.

2. **Supports:**

➔ **Fixed Support (E):** Fully constrained at the central hole, restricting all degrees of freedom.

Results Summary

1. Total Deformation

- **Maximum Deformation:** 0.00013105 m (0.131 mm)

➔ Located near the topmost edges of the structure where the forces are applied.

- **Minimum Deformation:** 0 m

➔ Found at the fixed support.

- **Interpretation:** The deformation is minimal, suggesting the structure exhibits high stiffness under the applied load.

2. Equivalent von-Mises Stress

- **Maximum Stress:** 287.58 MPa

➔ Concentrated near the top two loaded holes where stress concentrations are present.

- **Minimum Stress:** 169.35 kPa

➔ Spread across the bulk of the structure in low-load areas.

- **Interpretation:** High-stress regions indicate potential failure zones, requiring careful material selection or design adjustments. The stress values should be compared with the material's yield strength to ensure safety.

3. Equivalent Elastic Strain

- **Maximum Strain:** 0.0014409 mm/mm

➔ Found near the high-stress regions at the top holes.

- **Minimum Strain:** 1.7291e-6 mm/mm

➔ Found in low-stress areas across the body.

- **Interpretation:** The strain values confirm that the structure is operating within the elastic range, assuming a material with sufficient yield strain.

4. Mesh Quality

- **Mesh Distribution:** A fine mesh is employed around the holes and curved regions where stress and strain gradients are expected to be high.
- **Global Mesh Quality:** Adequate for capturing the behavior of critical regions, ensuring reliable results.

Outline of Schematic A2: Engineering Data

	A	B	C	D	E
1	Contents of Engineering Data			Source	Description
3	4130 Alloy Steel			C:\Users\student\Desktop\Upper Wishbone FEA_files\d	

Properties of Outline Row 3: 4130 Alloy Steel

	A	B	C	D	E
1	Property	Value	Unit		
2	Material Field Variables	Table			
3	Density	7.85	kg m^-3		
4	Isotropic Secant Coefficient of Thermal Expansion				
5	Coefficient of Thermal Expansion	1.12E-05	C^-1		
6	Isotropic Elasticity				
7	Derive from	Young's Mod...			
8	Young's Modulus	205	GPa		
9	Poisson's Ratio	0.29			
10	Bulk Modulus	1.627E+11	Pa		
11	Shear Modulus	7.9457E+10	Pa		
12	Tensile Yield Strength	435	MPa		
13	Compressive Yield Strength	435	MPa		
14	Tensile Ultimate Strength	670	MPa		
15	Compressive Ultimate Strength	670	MPa		

Figure C.28: Material Properties for Steel

Outline of Schematic A2: Engineering Data

	A	B	C	D	E
1	Contents of Engineering Data			Source	Description
2	Material				
3	6061 Aluminum			C:\Users\student\Desktop\Rocker FEA_files\dp0\SYS\ENGD\EngineeringData.xml	

Properties of Outline Row 3: 6061 Aluminum

	A	B	C	D	E
1	Property	Value	Unit		
2	Material Field Variables	Table			
3	Density	2.7	g cm^-3		
4	Isotropic Secant Coefficient of Thermal Expansion				
5	Coefficient of Thermal Expansion	1.31E-05	F^-1		
6	Isotropic Elasticity				
7	Derive from	Young's Modulus and Poiss...			
8	Young's Modulus	69	GPa		
9	Poisson's Ratio	0.33			
10	Bulk Modulus	6.7647E+10	Pa		
11	Shear Modulus	2.594E+10	Pa		
12	Tensile Yield Strength	40000	psi		
13	Compressive Yield Strength	40000	psi		
14	Tensile Ultimate Strength	45000	psi		
15	Compressive Ultimate Strength	45000	psi		

Figure C.28: Material Properties for T6 6061 Aluminum